



UNIVERSITAT
POLITÈCNICA
DE VALÈNCIA



FINAL YEAR INTERNSHIP

Coastal bathymetry from satellite high resolution monitoring

Javier SONES BORI

2017-2018

Confidentiality Notice: Non-confidential report

COMPANY	CNES, Legos
INTERNSHIP TUTOR	Philippe MAISONGRANDE
INTERNSHIP RESPONSIBLE	David MIMOUN
INTERNSHIP DURATION	April 2018 - September 2018
YEAR OF STUDIES	Master 2 in Aeronautical Engineering (UPV) ISAE-Supaéro, 3ème année (Erasmus+)

Confidentiality notice

This present document is not confidential. It can be communicated outside in paper format or distributed in electronic format.

To my parents

Acknowledgements

First of all I would like to thank Dr. Philippe Maisongrande the opportunity he has given to me to realize my Master Thesis in LEGOS by means of a CNES internship, for his great experience and patience.

Secondly I would like to thank Dr. Erwin Bengsma and Dr. Rafael Almar for all the things that I have learnt from them, for making me feel an important part of their team and for giving me the opportunity to work in their projects.

I would also like to thank all the people that I have met during this internship, the interns of LEGOS and CNES and, in general, all the people from both companies that gave me so many good moments.

A sincerely thanks is dedicated to all my friends and university colleagues which have helped me not only during the Master Thesis, but also during all my studies. To the ones that stay in Valencia and also to all the people that has made this year a great Erasmus experience.

And last but not least, thanks to my family for their unconditional support

Abstract

Bathymetry is traditionally obtained by echo sounding technology. However, bathymetry can be also obtained from satellite imaging, which is much more cheaper than echo-sound measurements. This is obtained by analyzing the waves near to the shoreline. In order so, wave properties such as wavelength and celerity should be measured, after which the bathymetry is estimated using linear wave theory. In this internship a new method based in the continuous wavelet transform has been implemented. In order to obtain the celerity, two images with a time lag are needed. Two data sets are used. On the one hand a video product, with 12 Pléiades images with a time lag between them of 8s. On the other hand a set of Sentinel-2 images. In the latter, a time shift between bands because of a lag in the acquisition is exploited. An application for the extraction and preparation of Sentinel-2 data in a form of a Graphical User Interface has been implemented. The site that has been studied will be the shore of Capbreton, which hosts one of the world's deepest canyons. The images have been be pre-filtered by using FFT and Radon filters, with several methods that include windowing of fixed and variable size. Those filtering techniques have be implemented and its results compared. Best results are obtained using a variable-size windowing technique. Finally, the wavelet method has been applied to both datasets to achieve wave propagation information.

Contents

1	Introduction	9
1.1	Context	9
1.2	Presentation of the company	9
1.2.1	CNES	10
1.2.2	LEGOS	10
1.3	Objectives of the internship	11
2	State of the art	12
3	Case of study	14
3.1	Satellites and image products description	14
3.1.1	Sentinel II	14
3.1.2	Pléiades	14
3.2	Site description	15
3.2.1	Capbreton, France	15
3.3	Data set	16
3.3.1	Pléiades data	16
3.3.2	Sentinel 2 data	17
4	Methodology	19
4.1	Sentinel 2 data extraction and preparation	19
4.2	Radon Transform filtering	20
4.3	Fourier Transform filtering	22
4.4	Land masking	24
4.5	Image filtering	24
4.5.1	Type of filters	25
4.5.2	Type of filter implementation	26
4.6	Limit setting of wavelet analysis	27
4.7	Wavelet analysis method and bathymetry extraction	28
4.7.1	CWT: 1D case	28
4.7.2	CWT: 2D case	29
4.7.3	Application to synthetic data	32
5	Results	35
5.1	Sentinel-2	35
5.1.1	Data pre-filtering	35
5.1.2	Wavelet analysis application and bathymetry inversion	37
5.2	Pléiades	39
5.2.1	Data pre-filtering	39

5.2.2	Wavelet analysis application and bathymetry inversion	40
6	Conclusions	42
7	Further work	43

List of Figures

3.2.1 Maps at 1/50000 : © Bourillet J-F. (Coord.), Augris C., Cirac P., Mazé J.-P., Normand A., Loubrieu B., Crusson A., Gaudin M., Poirier D., Satra C. and Simplet L. (2007). Capbreton canyon. morpho-bathymetric maps, Ifremer (Ed.) and Université Bordeaux 1.	16
3.3.1 Results for the phase difference and the translation calculation for the synthetic dataset.	16
3.3.2 Panchromatic image of the first date of Pléiades video product	17
3.3.3 Images of the 4 Sentinel-2 bands with 10m resolution in Capbreton	18
4.1.1 GUI for the extraction of SII data.	20
4.2.1 Representation of the Radon transform. Integration over all possible lines. Left: image space. Right: Radon space.	21
4.3.1 2D FFT of an ideal sinusoidal wave of 10m in a 200m image of 1m resolution . .	23
4.4.1 Land filtering of the Sentinel-2 and Pléiades data sets.	24
4.5.1 FFT mask.	25
4.5.2 Radon transform	26
4.5.3 Variable-size windowing filter process. Calculation of the distance to land of each point and setting of a window size.	27
4.6.1 Process to set the limits of the wavelet analysis. Application of the Radon transform to obtain the most important angle for each point, and histogram plot. . . .	28
4.7.1 Representation of a Morlet wavelet	28
4.7.2 Mother 2D Morlet wavelet with MATLAB default parameters.	30
4.7.3 Original synthetic image for the wavelet method validation.	32
4.7.4 Synthetic dataset for the wavelet transform method testing (close ups).	33
4.7.5 Magnitude of the complex CWT coefficients for the point [100,100] m.	33
4.7.6 Maps obtained with the application of the CWT to the synthetic data.	33
4.7.7 Results for the phase difference and the translation calculation for the synthetic dataset.	34
5.1.1 FFT and Radon filters to a whole Sentinel image without windowing.	35
5.1.2 FFT and Radon filters to a whole Sentinel image with fixed size windowing. . . .	36
5.1.3 FFT and Radon filters to a whole Sentinel image with variable size windowing. .	36
5.1.4 Radon filtering of Sentinel-2 image for each band. Comparison between red and blue bands to show the time lag. Zoomed to show it better.	37
5.1.5 Outputs of the Continuous Wavelet Transform application to Sentinel-2 images. .	37
5.1.6 Map of wave properties of Sentinel-2 images and depth inversion.	38
5.2.1 First Pléiades image of the video. Original and filtered.	39
5.2.2 First and second Pléiades images of the video with the FFT filtering. Zoomed view	40
5.2.3 Outputs of the Continuous Wavelet Transform application to Pléiades images. . .	40
5.2.4 Map of wave properties of Pléiades images and depth inversion.	41

Chapter 1

Introduction

1.1 Context

Coastal areas are very sensible to environment changes. In the recent days they are becoming more frequent, in such a way that they can change coastal bathymetry and shoreline in a very rapid way. The knowledge of the changes in bathymetry then becomes very important in order to prevent or mitigate the effects of those changes. In fact, the water depth near to the coast, in some regions, varies continuously. Some factors could be the incident waves, currents or the presence of a river near to the shore.

Traditionally, bathymetric data is obtained using ship-mounted echo sounding technology. However, the collected data usually covers some square kilometres, but the data are not usually collected in a daily basis. More recently, remote sensing techniques from satellite imaging, successfully obtained bathymetries through depth inversion. Bathymetry inversion through satellite images could be cheaper, easier and potentially real-time, as the whole world is sampled regularly. The bathymetry or depth can be obtained by looking at its effects in the wave properties. It's known that the slower the celerity, the shallower the waters, so that could be exploited to estimate the bathymetry.

Waves can be successfully extracted from satellite images. This is possible because of the specular reflection of the sunlight in the wave facets, which can make the waves visible in certain conditions. The wave visibility depends on the geometry of the instruments, the sunlight and if there are clouds or not. If the waves can be seen, then, wave properties such as wavelength and celerity can be extracted. In order to extract the wavelength, only one image is needed. However, in order to extract celerity, at least two images with a time shift between them is needed. Bathymetry can then be extracted using the well known linear dispersion relation of wave theory. It's based in the fact that, for intermediate sea depths, the bathymetry dictates the wave properties, so by knowing the wavelength and the celerity of the waves, the depth can be obtained.

1.2 Presentation of the company

This internship has been done in CNES (Centre National d'Etudes Spatiales) and LEGOS (Laboratoire d'études en géophysique et océanographie spatiales) in Toulouse France. Both companies will be presented.

1.2.1 CNES

Founded in 1961, the Centre National d'Etudes Spatiales (CNES) is the government agency responsible for shaping and implementing France's space policy in Europe. It conceives and executes space programmes with its partners in the scientific community and industry, and is closely involved in many international cooperation programmes.

The agency's more-than 2,400 employees, with some 1,800 engineers and executives. Its main activities are: Ariane, sciences, observation, telecommunications and defence

The CNES several tracking stations. Some of them are Kourou in French Guiana, Issus Ausaguel near Toulouse, Kerguelen Island, Hartebeesthoek in South Africa and Kiruna in Sweden.

CNES launches and uses some satellites for Earth Observation. The Pléiades programme was launched in October 2003 with CNES (the French space agency) as the overall system prime contractor. Moreover, Sentinel-2 data are also available through CNES's PEPS digital platform. CNES roles in Earth Observation are them both the launching of satellites and/or the use and distribution of its data.

1.2.2 LEGOS

LEGOS (*Laboratoire d'Etudes en Géophysique et Océanographie Spatiale*) is one of seven laboratories in the "Observatoire Midi Pyrenees" (OMP). It comprises personnel from four employing organisations: Centre National d'Etudes Spatiales(CNES), the national research organisations(CNRS, Département des Sciences de l'Univers), the Institut de Recherche pour la Développement (IRD) and the University Paul Sabatier (UPS). LEGOS has about 100 members: 40 researchers, 20 technicians and 30 postgraduate students and post-doctoral and contract staff. LEGOS is also houses the French Navy hydrographic and oceanographic service(CMO-Toulouse).

LEGOS is a multi-disciplinary research organisation, concerned with environmental research centred on physical oceanography (large scale and coastal), marine geochemistry and biogeochemistry, spatial hydrology and the dynamics of polar ice sheets. These research themes are linked by an observational approach using remote sensing from satellites. LEGOS is involved in all aspects of satellite missions, especially for altimetric satellites, from the planning and the preparation of algorithms to calibration, validation and exploitation of the results.

Besides, LEGOS contributes actively to student formation , and is involved in university teaching and supervision at all levels from degree to masters and PhD studies through the university faculties of physical science (UFR PCA), life and earth sciences (UFR SVT) and the doctoral school SDU2E (Sciences de l'Univers, Espace et Environnement).

The scientific activities at LEGOS are grouped into four themes [1]:

- Research in glaciology
- Research in hydrology and satellite-based geodesy
- Research in physical oceanography
- Research in marine biogeochemistry

1.3 Objectives of the internship

The objectives of this internship are multiple. This internship will show the application of new methods to the bathymetry extraction with satellite imagery, with two satellite products: Sentinel-2 and Pléiades.

First of all, the extraction of satellite images from databases available in the web will be automatized. An application for the extraction and preparation of data from the Theia database for Sentinel-2 images will be implemented. This will be useful to extract only the relevant data and provide it in a user-friendly way.

Secondly, a revision of the state of the art in wave enhancing in satellite images will be done, and some existing method and new methods will be implemented and compared. Some new filtering techniques will also be implemented and its effectivity will be shown.

Thirdly, a new method for bathymetry extraction from satellite images will be implemented, and tested in Sentinel-2 images and Pléiades images, obtaining then a resolution study. Bathymetry will be then compared to real bathymetry obtained by ship-mounted echo sounding technologies.

Ultimately the objective is to collaboratively write two papers that will be published in the near future.

Chapter 2

State of the art

Ocean waves are important for several reasons. For instance, ocean swell highly affects coastal areas, being one of the principal agents responsible for coastal erosion. Moreover, the spatial patterns of its frequencies and directions can provide information about bathymetry, that is, the ocean floor topography, at shallow depth. Some techniques to measure waves include in-situ measurements, which are accurate but lack from spatial range in the case of buoys, or temporal range in case of air-borne imagery [2].

Satellite imagery can be useful to overcome those deficiencies. Space-borne sensors capture the specular reflection of visible sunlight on the multiple facets of the ocean swell, and then the waves can be inferred for those images. Then, images from earth-observation satellites are useful to obtain the wavelengths and directions of waves in the moment in which the image is taken. This technique has some advantages:

- Access to remote areas with wide spatial coverage at high spatial resolution.
- Regular basis acquisition and data storage from the past
- Affordable cost

However, it has some disadvantages to:

- Wave celerity c cannot be directly measured.
- Ground calibration measurements are needed
- Limited by clouds, and to periods for which the sun, the sensor, and the ocean wave field are in a favourable alignment to allow for the swell image formation

Temporal frequencies of waves cannot be obtained by a single image, and then wave celerity cannot be obtained. There are some approaches to estimate them. First one involves to simply estimate the wave celerity from the linear wave theory. The celerity of is related with the bathymetry by the following formula:

$$h = \frac{1}{k} \tanh^{-1} \left(\frac{c^2 k}{g} \right) \quad (2.0.1)$$

where c is the wave celerity, k is the wave number, g is the gravity acceleration and h is the water depth, hence, the bathymetry. (2.3.1) is also known as the dispersion relation for surface gravity waves [3]. If bathymetry is unknown and the wave is far from the coastline, in deep water, the expression reduces to:

$$c_{deep} = \sqrt{\frac{g\lambda}{2\pi}} \quad (2.0.2)$$

Wave period can then be estimated directly by dividing the wavelength by the celerity. In order to obtain an acceptable celerity estimation in the case of an unknown bathymetry, an approximation from an estimation of wave celerity in pixels far from the coastline could be an option.

Recent methods have used the fact that some satellites which have multi-spectral and panchromatic sensors have a time lag between them. It is the case of SPOT-5 satellite images, separated by a time lag of 2.04 s or Pléiades images, with a lag of 0.16 s [4]. Even the Multi-Spectral Instrument of Sentinel 2 has lags between all these bands due to its geometry, with several values which can be found in the manuals. For example, between band 2 (blue) and band 3 (green) there's an offset of 0.527 s [5]. By finding how much a wave has moved from one image to the another one in terms of distance, and by knowing this time lag, the wave celerity can be directly inferred, as these lags are normally less than wave periods. These methods are also called Wave Kinematics Bathymetry of WKB [6].

Recently a method called CWB method for correlation, wavelets, and bathymetry has been proposed and applied to SPOT-5 images. A brief description of this method is now exposed. Cross-correlation is used to obtain the displacement between dominant waves. 2D continuous wavelet analysis is used to extract those dominant waves in every spatial point of the image. By finding which waves (wavelength and direction) are more energetic (higher values in the wavelet spectrum) and which ones correlate the best, a celerity field is obtained. The bathymetry is then obtained from the dispersion relation [4]. Morlet wavelets were applied to sub-scenes of variable dimension so that each sub-scene contains at least two wave crests and two wave troughs. In the study that was performed, the sub-scene sizes ranged from 640 m offshore to 320 m near-shore, on the basis that the more energetic wavelengths typically range from approximately 250 m offshore to approximately 100 m near the coast [3]. Wavelet analysis is considered to be well adapted in this case because it may be computed at each pixel, providing a precise value of the wavelength on these pixels.

In previous stages of the method a Fourier-filtered sub-scene was used to the cross-correlation instead of the real part of the wavelet transform, but it has been shown that wavelets are more powerful in this application. It's also proposed to use the phase information of a Short Time Fourier Transform instead of the cross-correlation to obtain the lag between a wave between the two images [6]. We can then also think about using sort of a phase information obtained from the imaginary part of the wavelet transform.

Another possibility for the estimation of the bathymetry is from video imaging. It has a great resolution, but it's limited to regions near the shore. Almar et al. [7] proposed a method using a time and space cross-correlation based on time-stack images, with very promising results. There are some other techniques in the literature for the extraction of wave characteristics, as the use of Complex Empirical Orthogonal Function (CEOF) analysis of intensity signal or individual wave front tracking. Bathymetry is then inverted from those characteristics.

Chapter 3

Case of study

3.1 Satellites and image products description

3.1.1 Sentinel II

Sentinel II is a European wide-swath, high-resolution, multi-spectral imaging mission, developed by ESA as part of the Copernicus Programme. Copernicus is the name for the Global Monitoring for Environment and Security programme, previously known as GMES. This initiative is headed by the European Commission (EC) in partnership with the European Space Agency (ESA) [8].

The Sentinel II constellation consists of two identical satellites, Sentinel-2A, launched on 23 June 2015, and Sentinel-2B, launched on 7 March 2017, flying in the same orbit but phased at 180°. The satellite lifespan is 7.25 years. The mission is designed to give a revisit frequency of 5 days at the Equator. Sentinel II satellites carry an optical instrument payload, the MSI (Multi-Spectral Instrument) with 13 spectral bands: four bands at 10 m, six bands at 20 m and three bands at 60 m spatial resolution. The orbital swath is 290 km, and it covers land surfaces from 56° S to 84° N, coastal waters, and all of the Mediterranean Sea. [9].

In our case, the finest resolution possible of 10 m will be used. which include: BLUE (band 2, centred at 490 μm), GREEN (band 3, centred at 560 μm), RED (band 4, centred at 665 μm) and VNIR band (band 8, centred at 842 μm). [9]

ESA's Sentinel-data policy is free and open, as data can be obtained freely. Sentinel 2 products are provided by the Copernicus Open Access Hub and are also available in the Theia Land Data Centre, which is a French national inter-agency organization designed to foster the use of images issued from the space observation of land surfaces.[10].

Theia distributes level 2A products. Level 2A products correct the data for atmospheric effects and detect the clouds and their shadows [10]. These are provided in tiles of 100km x 100 km, ortho-rectified. Masks are also be provided as products, including clouds, geophysical, edge, saturation, AOT masks, and a duplicate of the images with correction of slope effects [11].

3.1.2 Pléiades

Pléiades satellites provide images of a very high resolution, up to 50-cm resolution for standard ortho-products. The Pléiades satellites are designed to form a constellation of high resolution

satellites up to 2023, ensuring twice-daily revisit capability of high resolution images. This constellation is formed by:

- Pléiades 1A
- Pléiades 1B
- SPOT-6
- SPOT-7

In this case we will focus in Pléiades products. The Pléiades 1A spacecraft was launched on 17 December 2011 and Pléiades 1B on 2 December 2012. They provide the coverage of Earth's surface with a repeat cycle of 26 days, with a swath of 20 km.

The Pléiades panchromatic product covers wavelengths between 0.47 and 0.83 μm of the visible spectrum, with a pixel size of 0.5 m (Ortho-rectified). The multi-spectral product includes four bands: BLUE, RED, GREEN and NIR, with a pixel size of 2 m (Ortho-rectified). When the product is ordered, it can be received as a *bundle*, that is, the panchromatic and multispectral products, simultaneously acquired, are packaged together separately for a single delivery [12]. Pléiades products can be tristereo images, but ortho-rectified images will be used in this internship project.

Products are available to purchase in the Airbus Geostore [13], by demand.

3.2 Site description

3.2.1 Capbreton, France

As bathymetry influences directly on the wave dynamics, it's becomes interesting to study submarine structures with steep depth changes and near to shorelines. Capbreton's canyon is one of the world's deepest submarine structures [14]. It is located in the south-east of the Bay of Biscay, in the French south-west. It is a 300-kilometre-long meandering submarine structure that runs parallel with the north coast of Spain, before it curves northwards and disappears down the continental slope at a depth of 3500 m below sea level [15].

The canyon head forms a deep and wide structure facing out to sea, located only 250 m off the shoreline [15], near the beaches of Capbreton and Hossegor [14]. It is 1200 m wide in its shallower part (the headwall), and decreases to a width of 280 m as the canyon narrows with a steep slope around 4° in the shallow part and 8° in the deepest one [15].

Furthermore, its sedimentary activity leads to an important organic material transport to the depths of the canyon and, then, a great biodiversity [14]. In addition, its depth and configuration the canyon it a natural shelter from rough seas, as waves would surge by the shallower edges [16]. Environmental importance and the link between bathymetry and wave dynamics makes the Capbreton's canyon an interesting place to study.

The Capbreton coast is exposed to high energy North Atlantic swells travelling mainly from the W-NW sector (Butel et al., 2002), which generates a strong southward long-shore drift [15]. Dominant swells have a mean direction around 300° while less frequent wind seas have variable directions [17]. The mean annual frequencies range from $[4 - 22]$ s , the average frequency being

8 or 9 s, and mean amplitudes of 2 m. [18].

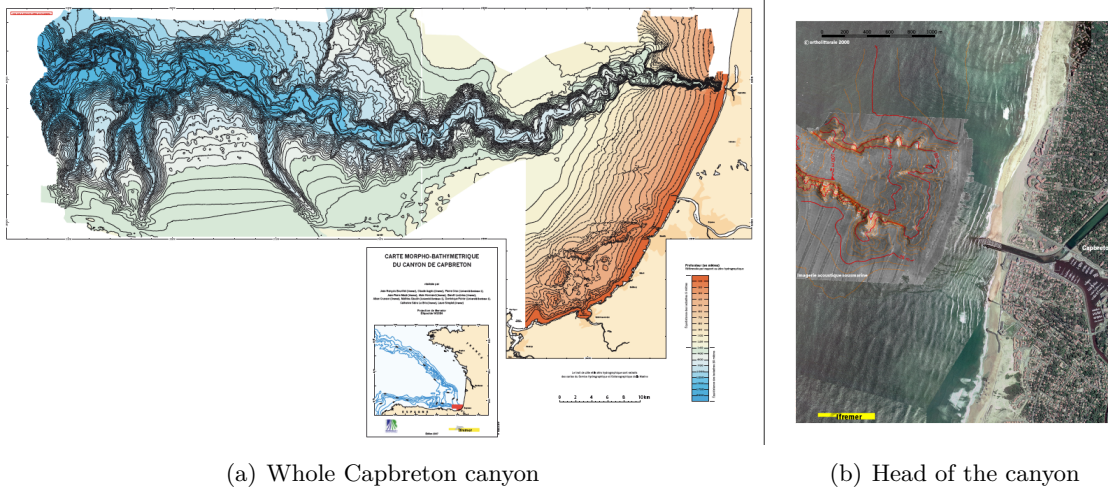


Figure 3.2.1: Maps at 1/50000 : © Bourillet J-F. (Coord.), Augris C., Cirac P., Mazé J.-P., Normand A., Loubrieu B., Crusson A., Gaudin M., Poirier D., Satra C. and Simplet L. (2007). Capbreton canyon. morpho-bathymetric maps, Ifremer (Ed.) and Université Bordeaux 1.

3.3 Data set

3.3.1 Pléiades data

The Pléiades data set consists in 12 images that form a video. The time shift between images is 8 seconds, so the wave propagation can easily be followed. The images that were taken are shown in Google Earth, in order to see its acquisition process.

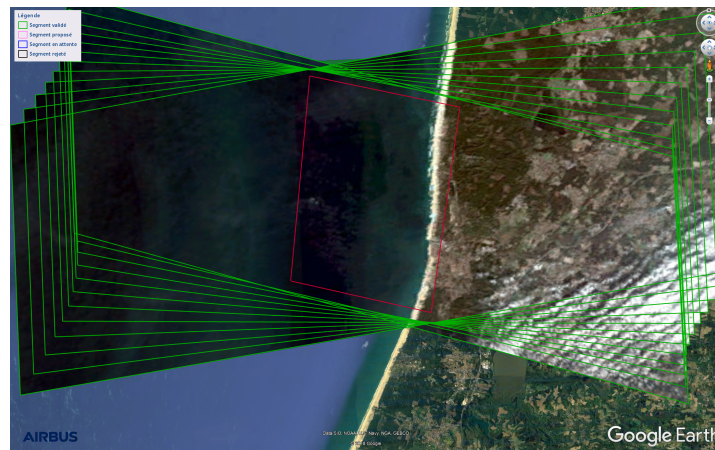


Figure 3.3.1: Results for the phase difference and the translation calculation for the synthetic dataset.

The coordinates of the images in Lambert 93 are:

- Nord-west corner: $X = 338000$; $Y = 6303000$

- South-east corner: X: 344000; Y = 6291500

The date of the first acquisition is the 18 November 2017, 11:04.

The image of the first image, in panchromatic, is shown in the next figure:

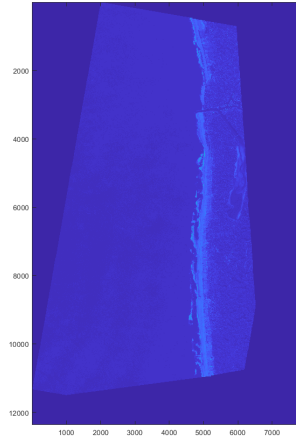


Figure 3.3.2: Panchromatic image of the first date of Pléiades video product

3.3.2 Sentinel 2 data

The Sentinel 2 data set is located in a sub-sample of the Pléiades data set that includes the river. 111 images of the scene are extracted from this scene, between the 30-Nov-2016 and the 23-Jun-2018. However, data are automatically filtered as there are some images with clouds or no data at all. This is done with the masks given by Theia. Finally, 26 dates are extracted. They are listed in the following figure:

Date list of the Sentinel 2 dataset in Capbreton		
30-Nov-2016 11:40:56	18-Jul-2017 11:44:58	20-Dec-2017 12:02:55
10-Dec-2016 11:50:59	02-Aug-2017 11:51:53	25-Dec-2017 11:43:56
29-Jan-2017 11:29:56	06-Sep-2017 11:12:55	15-Mar-2018 11:59:54
18-Feb-2017 11:11:56	11-Oct-2017 11:19:59	30-Mar-2018 10:59:55
10-Mar-2017 11:35:00	16-Oct-2017 11:30:58	14-Apr-2018 12:09:57
09-Apr-2017 11:51:51	26-Oct-2017 12:10:59	03-Jun-2018 12:13:59
19-Apr-2017 11:59:57	31-Oct-2017 11:19:58	08-Jun-2018 11:54:54
18-Jun-2017 11:40:54	20-Nov-2017 11:32:56	23-Jun-2018 11:51:54
28-Jun-2017 11:43:54	05-Dec-2017 11:41:56	

Table 3.3.1: Dates of the Sentinel-2 dataset

However, only the bands with best resolution are extracted. These are the optical ones and the near infra-red. The 4 bands for the 18th June 2017 are shown in the next figure.

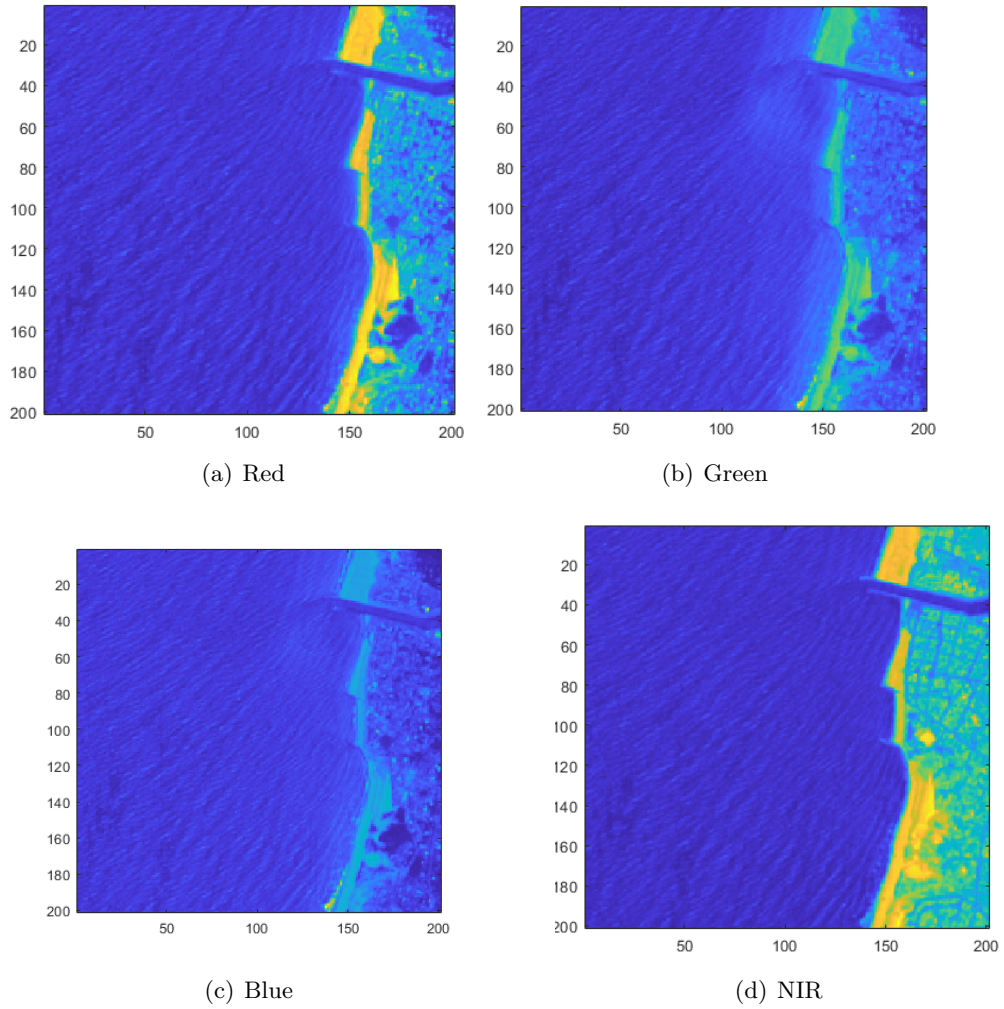


Figure 3.3.3: Images of the 4 Sentinel-2 bands with 10m resolution in Capbreton

The time delays between them are listed in the following table:

	Red	Green	Blue	NIR
Red	-	0.478 s	1.005 s	0.741 s
Green	-0.478 s	-	0.527	0.263
Blue	-1.005 s	-0.527 s	-	-0.264 s
NIR	-0.741 s	-0.263 s	0.264 s	-

Table 3.3.2: Time shift between bands of Sentinel-2 (positive sign:)

Chapter 4

Methodology

4.1 Sentinel 2 data extraction and preparation

Sentinel 2 images are downloaded from the Theia land data services centre website. A folder containing the date for one date and one tile will contain several files:

- The images of the 12 bands in GeoTIFF, with and without slope correction effects (12x2). The ones with 10 m will have 10980x10980 pixels, and then a tile size of 109.8x109.8 km
- A quicklook image
- A folder with all the masks (GeoTIFF), for example, a mask of clouds and their shadows, as well as a mask of water and snow
- A metadata file, containing informations like: coordinates, date, geometry (sun direction, incidence, etc.), and much more.

An extraction program is implemented in such a way that:

- Allows to extract a given date range
- Extracts the masks of interests, and with the option of adding them (and/or operations)
- Extracts only a window, defined by the coordinates of the upper-left and lower-right corner, in latitude/longitude or UTM.
- Indicates the data that are good (with no clouds and including real data, and not NaN).
- Does all this in a user-friendly way.

This program has been programmed as an interface (GUI) in MATLAB.

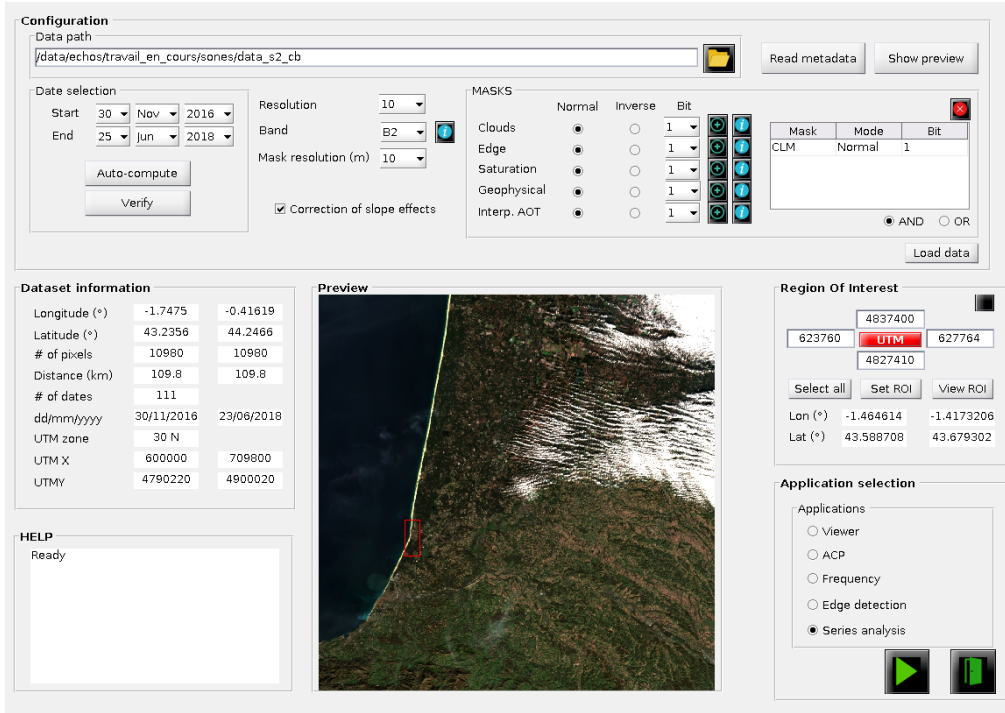


Figure 4.1.1: GUI for the extraction of SII data.

4.2 Radon Transform filtering

One of the filter that will be tested in this internship is based on the Radon Transform, so the basics of this transform will be explained. The Radon transform has a wide variety of applications in fields as engineering, medicine, and all areas of mathematics and the physical sciences. [19]. Radon transform, is well suited for line detection in digital images [20].

The Radon transform may be defined on various spaces of arbitrary dimension; however, for its application to images, it's enough to consider a two-dimensional Euclidean space [21]. The bi-dimensional Radon transform of a function $f(x, y)$ is defined as [22]:

$$R_f(\theta, \rho) = \int_D \int_D f(x, y) \delta(\rho - x \cos(\theta) - y \sin(\theta)) dy dx \quad (4.2.1)$$

where

- D is the entire image x-y plane,
- $f(x, y)$ is the image intensity (gray level) at position (x, y) ,
- $\delta(r)$ is the Dirac delta function which is zero except when $r = 0$,
- ρ is the length of the normal from the origin to the straight line,
- θ is the angle between the normal and the x axis.

The Radon transform accentuates linear features in an image by integrating image intensity along all possible lines in an image [22], defined by their offset ρ an angle θ . This can be shown in the following image.

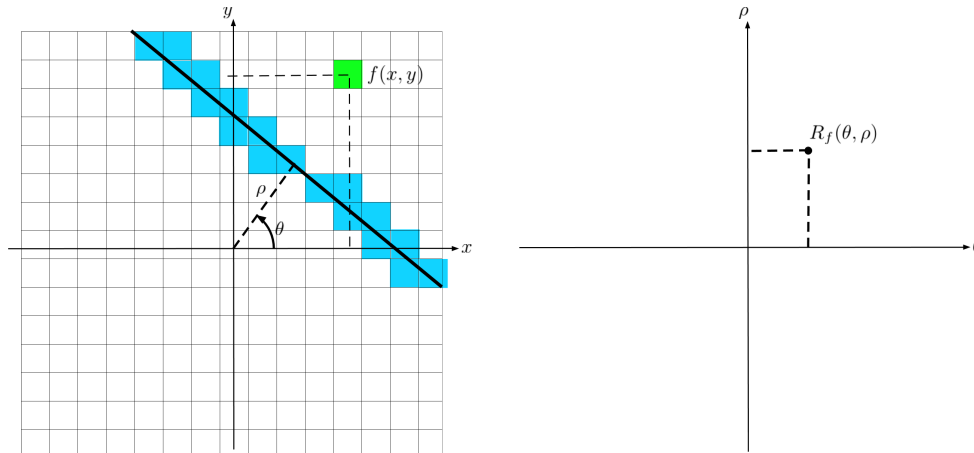


Figure 4.2.1: Representation of the Radon transform. Integration over all possible lines. Left: image space. Right: Radon space.

In recent years many algorithms for enhancing linear features in digital images have been suggested. Some of the alternative methods to the Radon transform found in the bibliography are listed:

- Method based on morphological operation, anisotropic Gaussian function and Hessian information [23].
- Canny edge detection [24].
- 2D Fourier Transform filtering
- Hough transform

One major advantage of the Radon Transform is that it can be applied to noisy images, as it's based in an integral technique and noise fluctuations tend to be cancelled. Moreover, this transform is invertible [25].

The Hough transform is closely related to the Radon transform, in fact, equivalent. In the Radon transform we consider how a data point in the destination space is obtained from the data in the source space: the reading paradigm. The alternative is to consider how a data point in the source space maps onto data points in the destination space: the writing paradigm of the Hough Transformation, even if it's always in a discrete setting. However, The Radon transform formalism has two advantages over the Hough formalism. It has a well-founded mathematical basis [26] and it's has more computational efficiency [23].

The 2D transform can be used to find the directions were predominant frequencies occur. It is not useful to find a single line, as it does not contain any periodicity. In the case of waves with associated wavelengths, Radon transform is more robust to enhance lines.

One deficiency of the Radon transform technique for line detection is that it cannot be used to detect linear features of dimensions much less than those of the image itself. However, a localized or windowed Radon Transform is used [25]. The Radon transform in a small window, enough to detect lines of a desired length, which can be shifted throughout the image. Some authors suggest that windows should overlap [22]. There's also artefact problems that can be

reduced by increasing the number of angular samples [25].

In Almar et al. [27] and Martins et al., 2017, the Radon transform is used to separate incoming from outgoing waves. It also can be useful to filter waves at a given direction. This is done by filtering the angles in the polar or Radon representation, and inverting to obtain the original signal. The advantage with respect to FFT filtering is the great angular resolution of this method. Here, the Radon transform will be applied for this purposes, as the objective is not to find the lines but to enhance it or, in other words, filter the lines in the directions that are irrelevant.

To increase the signal-to-noise ratio, a running mean filter was applied to the image data, by subtracting a local mean value from each pixel amplitude [28].

4.3 Fourier Transform filtering

Another filter that will be tested in this internship is based on the Fourier Transform, so the basics of this transform will also be explained. The Fourier transform is a mathematical transformation of a time-domain signal (or spatial-domain) into a frequency-domain representation by getting of a complex-value function, whose absolute value represents the amount of that frequency present in the original function, and whose complex argument is the phase offset of the basic sinusoid in that frequency. Mathematically, in its angular-frequency (ω [rad/s or rad/m]) convention, the Fourier transform $F(\omega)$ of a function $f(x)$, and its inverse transform, are defined as follows:

$$F(\omega) = \int_{-\infty}^{\infty} f(x)e^{-i\omega x} dx \quad f(x) = \int_{-\infty}^{\infty} F(\omega)e^{i\omega x} d\omega \quad (4.3.1)$$

For computational purposes, the Discrete Fourier Transform (DFT) is used. Let X be a discretized signal of length n and Y its DFT of the same length. The DFT and its inverse transform are then defined as:

$$Y(p) = \sum_{j=1}^n X(j)W_n^{(j-1)(p-1)} \quad X(j) = \frac{1}{n} \sum_{p=1}^n Y(p)W_n^{-(j-1)(p-1)} \quad (4.3.2)$$

where $W_n = e^{-2\pi i/n}$. In this notation it has been taken into account the MATLAB starts its indexing in 1. Then, the first value of Y , $j = 1$, will be the zero-frequency or constant component. In MATLAB, the functions $Y = \text{fft}(X)$ and $X = \text{ifft}(Y)$ use the well-known Fast Fourier Transform algorithm [29].

The inverse Fourier transform can be useful to filter certain frequencies by eliminating them from the frequency domain representation and using the inverse Fourier transform to obtain a filtered time (or spatial) domain representation.

As images are basically two-dimensional signals, a 2D Fourier Transform can also be defined. The 2D DFT of a discrete function $f(m, n)$ and its inverse are defined as:

$$\begin{aligned}
Y(p, q) &= \sum_{j=1}^m \sum_{k=1}^n X(j, k) W_m^{(j-1)(p-1)} W_n^{(k-1)(q-1)} \\
X(j, k) &= \frac{1}{nm} \sum_{p=1}^m \sum_{q=1}^n Y(p, q) W_m^{-(j-1)(p-1)} W_n^{-(k-1)(q-1)}
\end{aligned} \tag{4.3.3}$$

where $W_m = e^{-2\pi i/m}$ and $W_n = e^{-2\pi i/n}$. In MATLAB, a 2D FFT is represented by the concatenation of two Fourier transforms. This is implemented in the function $Y = \text{fft2}(X) = \text{fft}(\text{fft}(X) \cdot \text{'}) \cdot \text{'}$ and $X = \text{ifft2}(Y)$. This 2D transform will give us the horizontal and vertical frequency contents or, which can be translated into a normal frequency and a direction.

An example is shown now to give the reader a clearer understanding in Figure 4.7.2. We generate an image with an ideal sinusoidal wave, with a wavelength of 10m and a direction of 45° from the horizontal. The absolute value of the FFT has been represented, shifting the function in such a way that the zero-frequency appears at the centre of the image with `fftshift`. In this case this value is non-zero, because we have shifted the sinusoid by a value of 0.5 in order to see this constant value. Moreover, two symmetrical peaks are obtained, which are 14 pixels horizontally and 14 pixels vertically from the centre. The number of points of the FFT is the same as the original image, and the pixel size of both images is related. The pixel size of the image is 1m, as the resolution is metric, so the sampling frequency is $F_s = 1 \text{ sample}/m$. The pixel size of the FFT is, then, $F_s/n = 1/200$ (in both dimensions), being n the number of pixels of the considered dimension; and the pixel size in units of m^{-1} . The distance in pixels between the peak and the centre is $\sqrt{14^2 + 14^2} \approx 20$, so the wave number and the wavelength will be:

$$k_x = k_y = 14 \cdot \frac{1}{200} \rightarrow k = \sqrt{k_x^2 + k_y^2} \rightarrow \lambda = \frac{1}{k} \approx 10m \tag{4.3.4}$$

And the angle:

$$\theta = \arctan\left(\frac{k_y}{k_x}\right) = 45^\circ \tag{4.3.5}$$

Showing a perfect relationship between frequency and time domain.

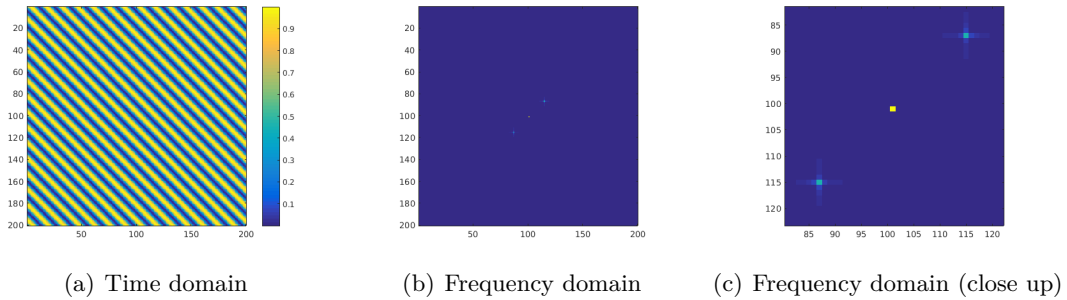


Figure 4.3.1: 2D FFT of an ideal sinusoidal wave of 10m in a 200m image of 1m resolution

In non-ideal waves, there are frequencies that are non relevant and/or confusing, so those can be filtered directly in the frequency domain by putting zeros in the desired frequencies-directions, getting a cleaned signal by using the inverse FFT. Some ideas for the filters are listed as follows:

- Filter a range of frequencies
- Filter a range of directions
- Choose a frequency-direction combination that is relevant by selecting a threshold or a single maximum value and filter everything else

4.4 Land masking

The filtering of the land is paramount to obtain good results near the coast, as its brighter pixels can influence the neighbouring sea pixels. It will also be useful to calculate the distance to the land from every point in the water. Land filters are introduced by using the different channels of Sentinel-2 and Pléiades.

- For Sentinel-2, the NDWI index has been calculated. It is defined as follows:

$$NDWI = \frac{Blue - NIR}{Blue + NIR} \quad (4.4.1)$$

- As for Pléiades images the infra-red channel is not available, we use a relation between the Green and Red channels, as follows:

$$Index = \frac{Red}{Green} \quad (4.4.2)$$

The filters in two image are shown in the next figures:

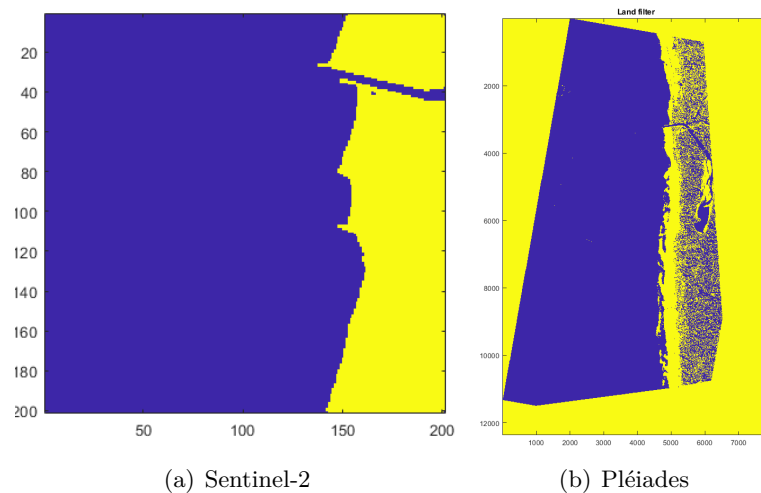


Figure 4.4.1: Land filtering of the Sentinel-2 and Pléiades data sets.

4.5 Image filtering

Once it is stated that the filters are based on the FFT and Radon transforms, some different filtering implementations will be tested.

Images from satellites do not show clear waves without preposition. This is due to noise and several components that worsens the clarity of wave identification. Some filters can, then,

be applied in order to show the waves. Here, FFT and Radon filters will be applied, as both filters allow for wavelengths and directions in the first case and only directions in the second case. They will be applied in windows, so two filtering methods will be implemented.

4.5.1 Type of filters

FFT filtering

The 2D Fourier transform allows us to filter an image in frequency and direction. The combination of the frequency and direction masks is shown in the following image:

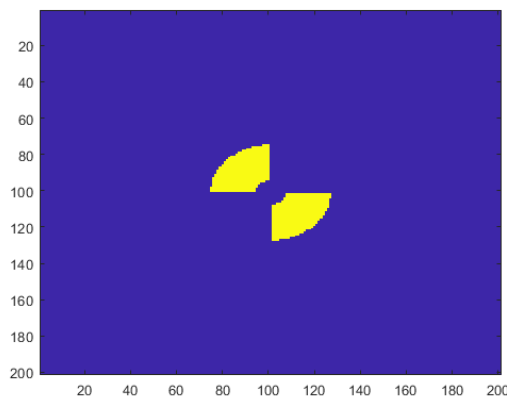


Figure 4.5.1: FFT mask.

The wavelength range is set in order to match the range of swell waves: between 7-8 and 25 seconds. By using linear wave theory in deep water, this period range can be translated into a wavelength range. The following relation have been used:

$$\lambda = \frac{gT^2}{2\pi} \quad (4.5.1)$$

The direction range is implemented in such a way that the range contains the most relevant FFT coefficients. This can be calculated by finding which coefficients are higher than a threshold, and setting the range in such a way that they are included (with a margin). Another option could be to calculate the quadrant in which the waves move (from south to north or vice versa), by comparing the coefficients in one quadrant with the coefficients in another one. Even if this method is simpler son but less applicable to special cases, for Capbreton is very useful as the swell waves seem to move in the same quadrant. However, the algorithms of the first method are also provided in order to apply the method to other regions.

Radon filtering

The Radon transform provides a polar representation of an image, as it has been shown in other sections. Its results are very useful in order to mask irrelevant angles. The Radon transform increases the signal-to-noise ratio because of its integration process, leading to noise reduction. The angles are filtered in the Radon space and, after applying the inverse Radon transform, the filtered image is obtained. In the next image an example of the Radon transform applied to a Sentinel-2 image is shown.

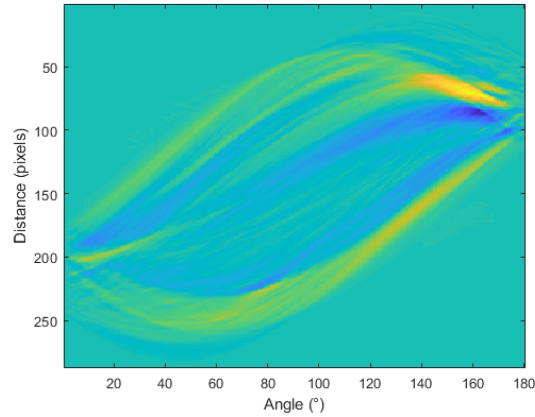


Figure 4.5.2: Radon transform

The only range to define for the radon transform is the angle range. One option is to apply it to a quadrant to extract only the incoming waves [27]. Another option could be to find the angle for the maximum coefficient and set a margin in order to define a range. The first will be applied as it has been demonstrated to be useful.

4.5.2 Type of filter implementation

No windowing

These filters can be applied directly to the images without no windowing at all. However, they produce inaccurate results specially in the borders of the image.

Fixed-size windowing

The recommended window size in this applications is one that allows to enclose two crests of wave in the image. Then, the windows can be applied with or without overlapping. Some overlapping is recommended in order to avoid innacurate results in the borders of the windows, as they will be compensated.

Variable size windowing

Filtering near to the land or objects like boats can produce bad filtered images in the windows that encloses a part of them. Then, a method has been implemented in order to avoid it. The window size is set to depend on the proximity to the land, in such a way that it increases as we are further from the coast, avoiding that the windows include the land. The proximity to the land or ships should be calculated. A method based on morphological operations have been applied. The operation that has been applied is dilatation, with a structuring element of 1 pixel. The algorithm sequence is as follows:

- A binary image in which 1 represents the land and 0 represents the water is obtained.
- The binary image is dilated, obtaining a new image which seems to have more land (as if the sea level had decreased).
- Both images are subtracted, obtaining the pixels with distance equal to one.

- The process is repeated until the whole image is dilated (all ones) or the dilatation reached a pre-defined limit.

A function defining the relation between the distance to the land and the window size has to be defined. In this case, the function will be:

- Increasing linearly at a given rate as the distance increases (recommended rate = 1/2)
- Equal to a maximum window size at distances higher than the ones that would produce windows sizes greater than the maximum ones (saturation)

In the following images, a distance map for a Sentinel-2 image and the function that relates window size with distance to land (or border) image are shown.

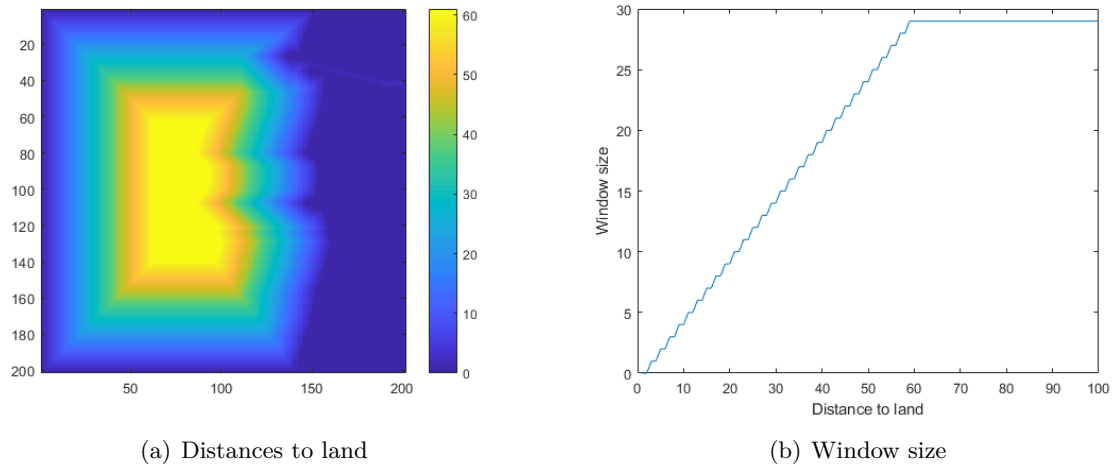


Figure 4.5.3: Variable-size windowing filter process. Calculation of the distance to land of each point and setting of a window size.

Every tile is added to the image as is we added patches. Finally, the image resulting of the sum of all patches will be normalized, point by point, by the times that the Radon transform has included this point, resulting in the final filtered image.

4.6 Limit setting of wavelet analysis

In the wavelet analysis, a range of frequencies and scales or wavelengths is required. As we do not want to calculate all possible values, but only the relevant ones to avoid unnecessary and slow calculations, an analysis should be performed in order to find these values.

In our case, the wavelength range is set with the help of wave theory. Nevertheless, the angles are calculated with the Radon transform. While the filtering is done, the angles in which the maximum Radon coefficients appear are saved. Then, we obtain a map of principal directions. This map is then translated into a histogram, obtaining a distribution in which the mean will represent the most relevant angle. The standard deviation can also be obtained. The range of the wavelet transform in angles will be set as an interval of confidence 1-sigma, meaning/ $[\theta_{mean} - \sigma, \theta_{mean} + \sigma]$. This process is shown in the following images:

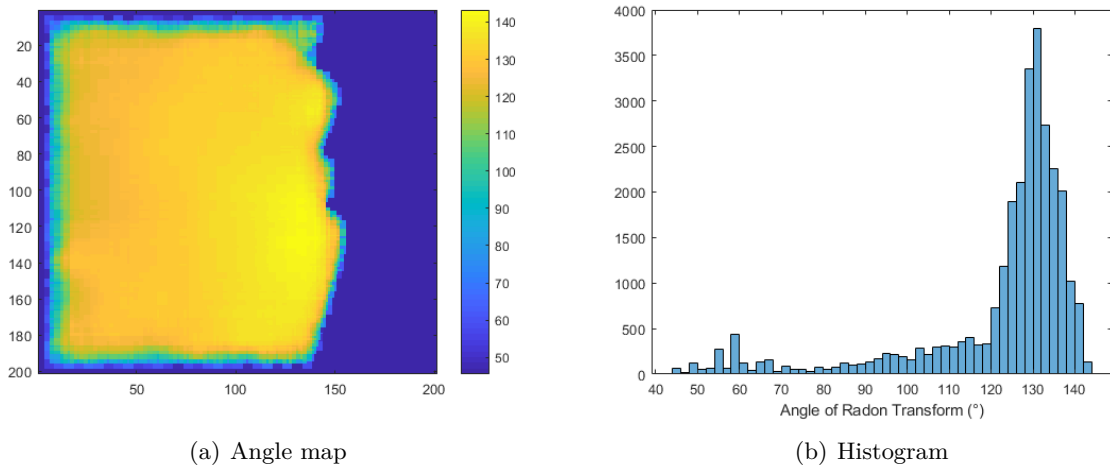


Figure 4.6.1: Process to set the limits of the wavelet analysis. Application of the Radon transform to obtain the most important angle for each point, and histogram plot.

4.7 Wavelet analysis method and bathymetry extraction

4.7.1 CWT: 1D case

In the Fourier representation, the resulting transform is only a function of the frequency, so the spatial or temporal domain is not represented. Then, with a simple Fourier transform we can't obtain a spatial evolution of a frequency, what it's called a spectrogram. One method to provide the localization of frequencies is to apply this transform in windows, the short-time Fourier transform (STFT). The tradeoff between time and frequency resolution is determined by the choice of the window function. In STFT one particular size of the time window is selected for all the frequencies, which restricts the flexibilities. Wavelet transform, however, can produce the same frequency-space domain with variable-sized regions, by allowing longer time intervals where more precise low-frequency information is required and shorter ones when high-frequency information is required [30]

Whereas in FFT the analysing function was a wave, in Continuous Wavelet Transforms (CWT) the analyzing function is a wavelet. A wavelet function $\psi(x)$ is some function which starts and ends in zero (space-localized), with zero mean and which is normalized [31]. There are several commonly used wavelets in the literature, but here we're going to use one of the simpler ones: the Morlet wavelet, which is the result of a multiplication between a sine wave (complex-exponential as we have to consider the imaginary plane too) and a gaussian.

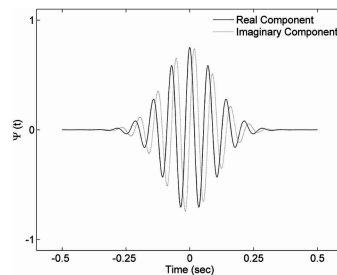


Figure 4.7.1: Representation of a Morlet wavelet

Then, translation can be applied in order to localize the wavelet in space (parameter u) and scaling (parameter s) to the mother wavelet like the Morlet one, as follows:

$$\psi_{s,u}(x) = \frac{1}{\sqrt{s}} \psi\left(\frac{x-u}{s}\right) \quad (4.7.1)$$

In the case of the Morlet wavelet, the scaling parameter is directly related to its frequency. The idea of the CWT is to find the correlation between the function and all possible scaled and translated wavelets, obtaining a space-frequency diagram. Mathematically, the 1D CWT of a function $f(x)$ is defined as follows [32]:

$$W_f(s, u) = \int_{-\infty}^{\infty} f(x) \psi_{s,u}^*(x) dx \quad (4.7.2)$$

where the asterisk refers to the complex conjugate. As images are 2D functions, we can define also a 2D CWT. In order to do that, we need four parameters for the wavelet:

- Translation in x , u_x
- Translation in y , u_y
- Scaling (proportional to frequency), s
- Rotation (direction, as in the 2D Fourier Transform), θ

The transformed wavelet is then defined as:

$$\psi_{s,\mathbf{u},\theta}(\mathbf{r}) = \frac{1}{s} \psi\left(R_\theta^{-1} \frac{\mathbf{r} - \mathbf{u}}{s}\right) \quad (4.7.3)$$

where \mathbf{r} is the (x,y) position, R_θ a rotation matrix and $\mathbf{u} = (u_x, u_y)$ [33]. The 2D CWT, by applying the Plancherel's theorem, is then defined as:

$$W_f(s, \mathbf{u}, \theta) = \int_{\mathbb{R}^2} f(x) \psi_{s,\mathbf{u},\theta}^*(\mathbf{r}) d\mathbf{r} = \int_{\mathbb{R}^2} \widehat{f}(\omega) \widehat{\psi}_{s,\theta}^*(\omega) e^{i\mathbf{u}\omega} d\omega; \quad \widehat{\psi}_{s,\theta}^*(\omega) = a\widehat{\psi}[aR_\theta^{-1}(\omega)] \quad (4.7.4)$$

where $\widehat{(\cdot)}$ states for the Fourier transform. The MATLAB function `cwtft2` computes the 2D CWT function by using a Fourier transform-based algorithm in which the 2-D Fourier transforms of the input data and analyzing wavelet are multiplied together and inverted [34].

4.7.2 CWT: 2D case

The Continuous Wavelet Transform has been used to obtain the wavelengths, directions and phases of the waves at each point of the image. This very useful to the analysis of waves by several reasons. First of all, the wavelet transform gives an spectrum at every point of the image. The method can explained, *grosso modo*, by localizing, scaling and rotating a wavelet, so the localization can be done for each point and the resolution will be the same as the original image. Besides, the wavelet can be scaled by differentials, meaning that all wavelengths can be tested, so if the wavelet method were perfectly applied the wavelength error would be around 1 m for the Pléiades images and 10 m for the Sentinel-2 ones. The same happens to the rotation of the wavelets, so all possible directions can also be tested.

First of all, the mother wavelet should be defined. A mother wavelet is the one with unitary scale and no translation nor rotation. In this case, a Morlet wavelet will be used. This wavelet

is composed of a complex exponential (carrier), which is a cosine in its real part and a sine in its imaginary part, multiplied by a Gaussian window (envelope), as it has been already explained in the previous section. One of its major advantages for our application is its symmetry, simplicity and frequency properties. In fact, it can be seen

$$\psi_M(\mathbf{x}) = \exp(j\mathbf{k}_0\mathbf{x}/\sigma) \exp\left(-\frac{1}{2}|A\mathbf{x}/\sigma|^2\right) \quad (4.7.5)$$

where \mathbf{x} is the 2D position, $\mathbf{k}_0 = [\omega_0, 0]$ and $A = \text{diag}(\epsilon^{-1/2}, 1)$. We can see that the first exponential corresponds to the complex carrier, and the second one to the gaussian window. The parameter ω_0 controls the frequency, σ the width of the gaussian window and ϵ defines the anisotropy of the gaussian filter, or in other words, i.e, its elongation in any desired direction. In our analysis, the default values are used: $\{\omega_0 = 6, \sigma = 1, \epsilon = 1\}$. The mother wavelet is defined as:

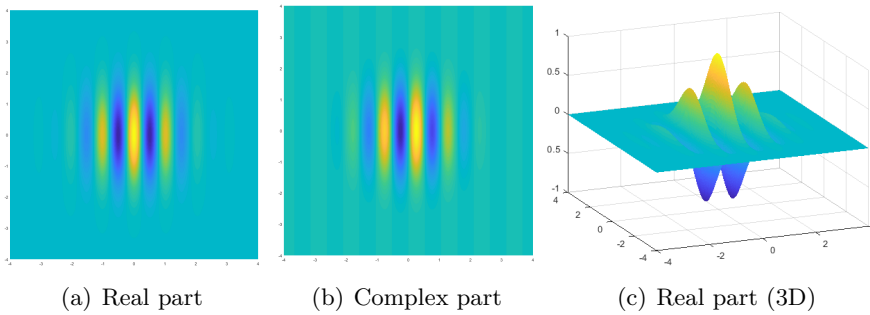


Figure 4.7.2: Mother 2D Morlet wavelet with MATLAB default parameters.

The central frequency of this wavelet is calculated with the help of MATLAB specific functions and it is equal to $f_W = 0.9750$. As the scale parameter s increases, the frequency of the wavelet respect to the mother wavelet decreases in the following way: $f = f_W/s$. The wavelength is, then proportional to the scale, so both concepts can be used in the same way.

The computational speed of the CWT is high. For the Pléiades images that are analysed here, the method takes around 20 minutes in a PC to calculate the CWT of a single image, which is considerably fast if it is considered that the image size is in the order of GB. However, the matrices that result from its calculation can be enormous. In fact, for each point of the image (x,y) we will have an spectrogram with the CWT coefficients for each angle and scale (or wavelength) that we want to analyse. That would give us 4-D matrices, (x, y, θ, λ) , that in some cases could be bigger than the maximum size allowed by MATLAB, if the image size is big or the angles and wavelengths ranges are big (or their resolutions small). Some strategies to solve this problem are:

- Define a smaller range of angles or wavelengths. This can be done with a previous FFT, the Radon transform or wave theory (described later)
- Reduce the resolution of the angles or wavelengths (instead of calculating for each one, calculate bigger steps)
- Calculate the CWT in tiles that allow the calculation.
- Implement the algorithm in such a way that the CWT is calculated angle-by-angle and/or wavelength-by-wavelength.

A combination of all the options has been applied.

For each point, the spectrum is calculated. After, the most relevant wavelengths and angles of the spectrum are extracted. The most relevant wavelengths means most energetic in this case, being them the one with highest absolute value of the complex coefficients (peaks in the spectra). In an ideal case, the maximum value of these coefficients will give the instantaneous wavelength and direction; if there's only one peak. However, it could be the case that more than one peak and, then, more than one wavelength-direction combination can be found. In order to select the correct one, some strategies could be used.

- Suppose that the maximum peak is the relevant one
- Extract several peaks (several wavelength-direction pairs for each point)
 - Take the points with only one peak as true wavelength-direction pairs, and for other points, take the pairs that give smoother distributions
 - Filter some peaks by applying wave-physics

Here, only the maximum peaks will be extracted, to show if the method is robust without additional hypothesis. However, the programming for the other options have also been implemented so that, if needed, it can be applied.

If two images are taken with a given time shift Δt , the displacement of the wave at each point and, then, the celerity can be obtained if the time lag between the two images is known. If the CWT method is applied independently to the two images, the wavelength maps that are obtained could vary between the images. Even if the difference will not be great, those little variations could worsen the validity of the results, as the method can only be applied if the same wavelengths and angles are considered for every point between the two images. Then, the approach is the following one:

- One of the images, that could be image that better shows the waves, is taken as the *base*. Then, the algorithm that finds the peaks in the CWT spectrum is applied and a map of wavelengths is obtained.
- For the second image, the CWT is calculated only for the wavelengths and directions of each point, so the wavelength and angles map will be the same as the first image but the coefficients will vary. Even if the maxima are not taken, the results will be more valid as they will be coherent with wave physics.

Once the CWT phase is calculated at each point (complex phase of the CWT coefficients), a phase difference $\Delta\phi$ can be calculated. Then, the wave displacement is a function of this phase difference and the wavelength, in the following way:

$$\Delta x = \lambda \frac{\Delta\phi}{2\pi} \quad (4.7.6)$$

The celerity at every point can be obtained as:

$$c = \frac{\Delta x}{\Delta t} \quad (4.7.7)$$

Finally, the bathymetry is extracted by using the dispersion relation:

$$h = \frac{1}{k} \tanh^{-1} \left(\frac{c^2 k}{g} \right) \quad (4.7.8)$$

where h is the depth, k the wave number, c the celerity and g the gravity acceleration. For the Pléiades product, the time lag of 8s between each frame of the video will be used, and for the Sentinel-2 images, the time lag between bands will be exploited. In this case, the BLUE and RED bands will be used, as their lag is the greatest among all the possible ones.

4.7.3 Application to synthetic data

In order to test the method, let's consider a synthetic case with real world properties such as wave shoaling. The generation of synthetic data can then be very useful. In this case, a signal that could represent a wave evolution is a chirp, a periodic signal with a frequency increasing in time (or space). This is generalized in 2D, and the signal is then rotated a given angle. Three 2D signals or images are generated:

- Original image, with 1000x1000 points, an angle of 60° and a wavelength varying from 10 to 20 m.
- Phased image, which will be the original image but with an initial phase ϕ_0 (rad) with respect to the original.
- Translated image, which will be the original image with a translation (in m) in the direction of propagation.

These images are shown in the following figures. As both three look very similar in the whole domain, the comparison between them is done in a sub-sample.

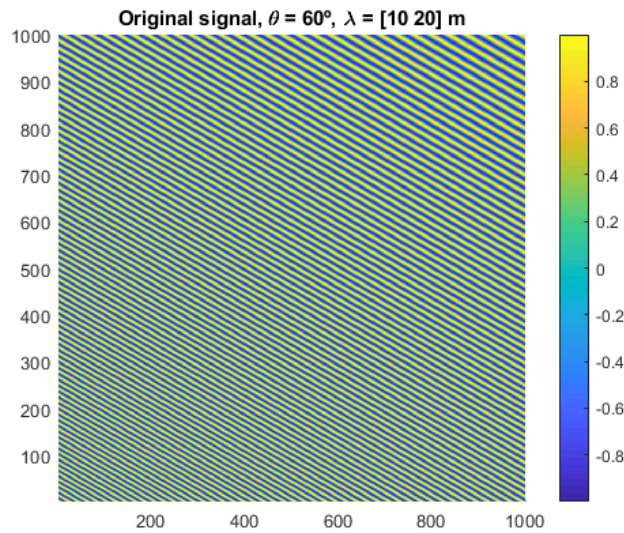


Figure 4.7.3: Original synthetic image for the wavelet method validation.

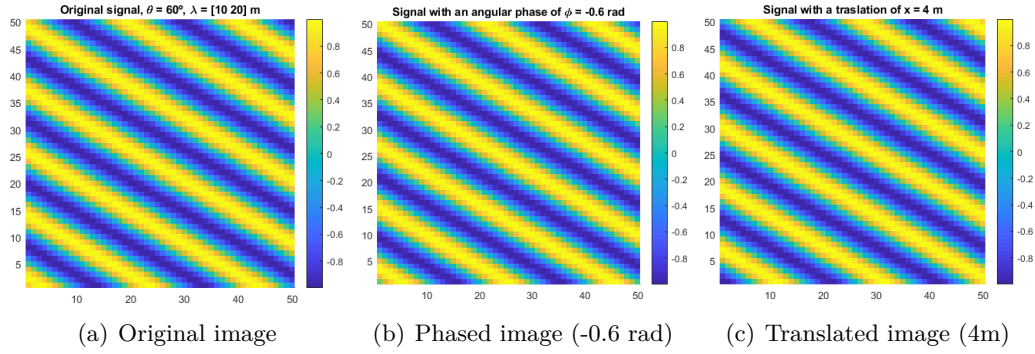


Figure 4.7.4: Synthetic dataset for the wavelet transform method testing (close ups).

Now the CWT method is applied, obtaining the complex coefficients for each point, angle and wavelength. The maximum coefficient (in magnitude) for each point is taken, as it's shown in the following figure.

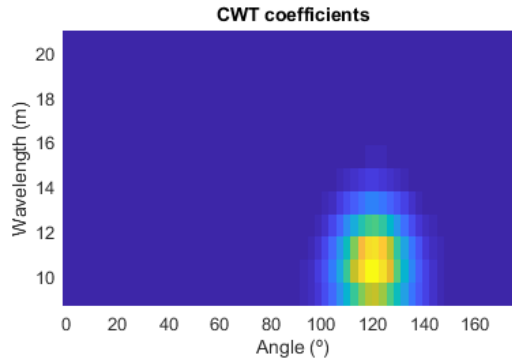


Figure 4.7.5: Magnitude of the complex CWT coefficients for the point [100,100] m.

In this case there is only one peak in the spectrum. Then, by taking these maximums, the maps of wavelengths, angles and complex phases (argument of each maximum complex coefficient) are obtained and shown in the next images.

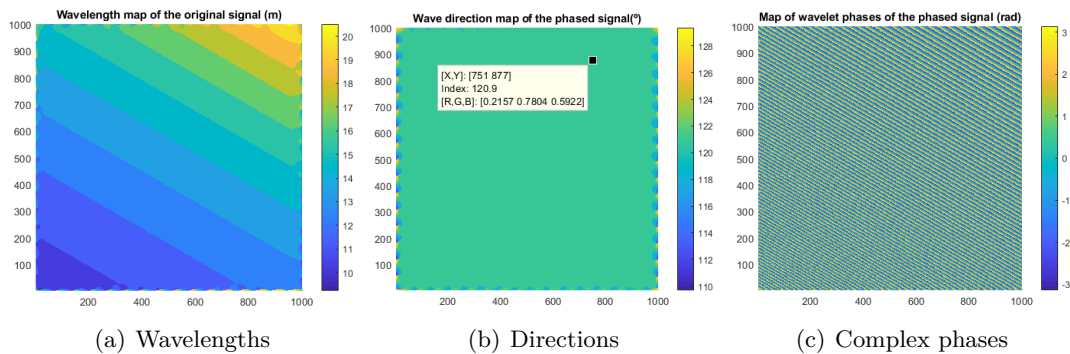


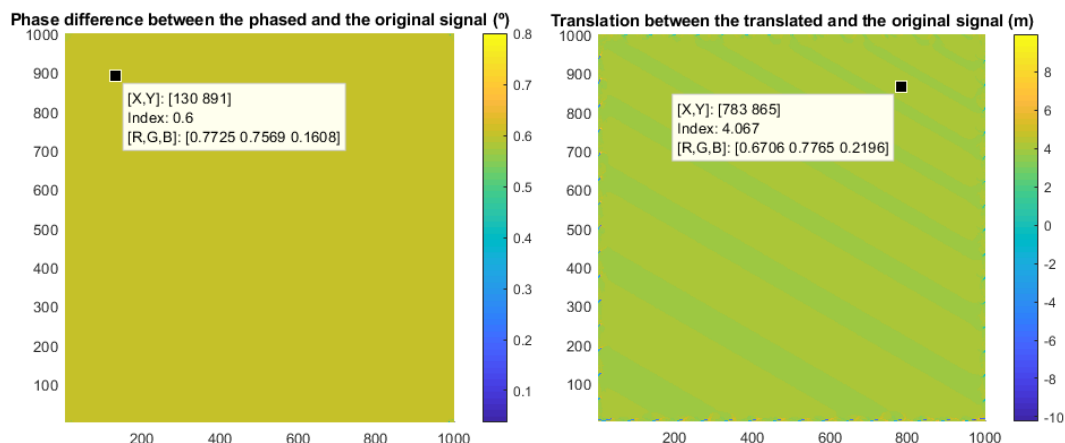
Figure 4.7.6: Maps obtained with the application of the CWT to the synthetic data.

The results for the wavelengths and angles are the ones that can be expected from the synthetic data generation. The complex phase looks so much like the wave, but its values varies from $-\pi$ to π . In fact, the phase equal to zero corresponds to the crests of the wave, and

the through to $\pm\pi$. This phase can be, then, used as a wave reconstruction. Moreover, if two images are compared, a phase difference $\Delta\phi$ can be obtained at each point. The translation Δx between these images at each point could be then calculated by knowing those phase differences and the wavelengths λ , by using the following relationship:

$$\Delta x = \lambda \frac{\Delta\phi}{2\pi} \quad (4.7.9)$$

The result are finally shown in the following figures, where there's an exact match between the input parameters and the wavelets results.



(a) Phase difference map for the original-phased image pair (b) Translation map for the original-translated image pair

Figure 4.7.7: Results for the phase difference and the translation calculation for the synthetic dataset.

The translation maps can be used to calculate the celerity, if we are comparing to images with a time delay. It is apparent that the wavelet analysis is powerful for the case of ideal waves, and the resolution of the wavelengths, angles and translations can be as low as what the image resolution allows. In the next sections this method will be applied to real data.

Chapter 5

Results

5.1 Sentinel-2

5.1.1 Data pre-filtering

The filters have been tested in the Sentinel-2 images. In order to avoid showing the results of all bands for all dates, only one image of the Blue band of the 18-Jun-2017 will be shown.

The results of the Radon and FFT filters without windowing are shown in the next figure.

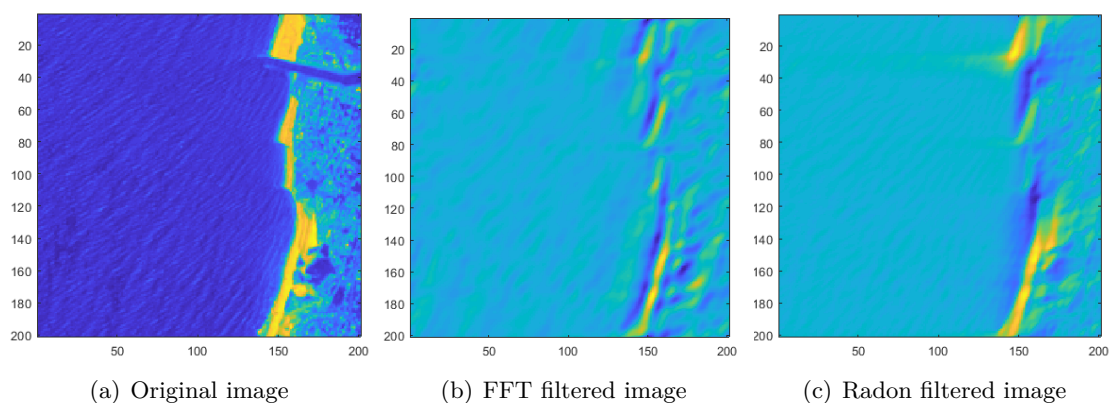


Figure 5.1.1: FFT and Radon filters to a whole Sentinel image without windowing.

These filters don't produce a great improvement of the original image. In fact, they produce artefacts that could worsen or make even impossible the wavelet method, as the CWT could take those artefacts as dominant waves. Now, a windowing with fixed size is applied.

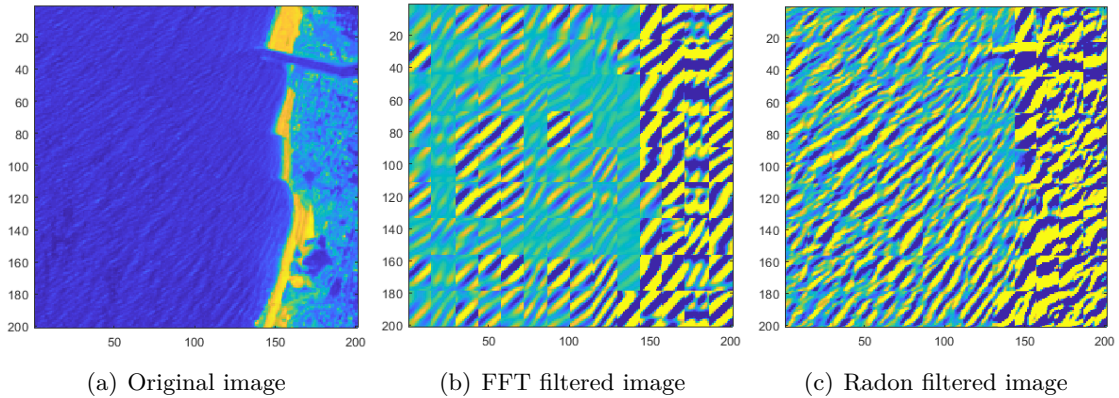


Figure 5.1.2: FFT and Radon filters to a whole Sentinel image with fixed size windowing.

In this case, the results for the FFT filtering are even worse, the tiles don't necessarily match because the FFT has not been normalized. However, even if it were normalized, it can be seen a tiling effect, that is, a difference in phase between two tiles at their junction. Moreover, near to the shore, the results would also be influenced by the land, as some tiles include it in their calculation. Even if the land were filtered, those tiles would show the effect of this filtered land, so the results near to the sea would not be correct. Finally, a windowing with variable size, with a window size smaller near to the land or the image borders is applied, and the results are shown in the next figure.

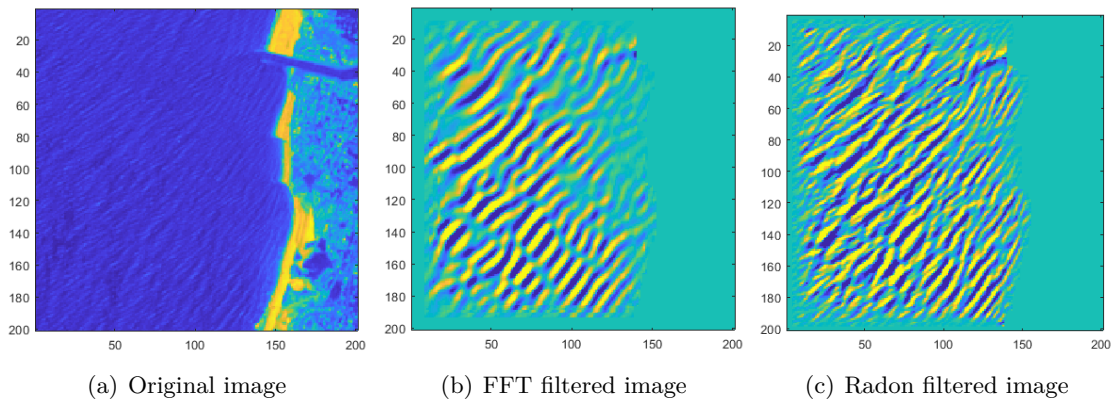


Figure 5.1.3: FFT and Radon filters to a whole Sentinel image with variable size windowing.

In this case, it can be seen that the effect of the tiles is not there any more, as they overlap. Furthermore, the results near to the land are now valid, as the tiles do not include it. The results between the FFT and Radon filter are very similar, although in the FFT filter the wavelengths are also taken into account, so the higher frequency waves are filtered and the image is cleaner.

Finally, a sub-sample of the Radon filtered image (with variable-size tiles) is shown in the next figure in order to verify that there is a lag between the the red and blue bands, as the lag is the greatest. The advancing of the wave can be observed if the images are carefully analysed).

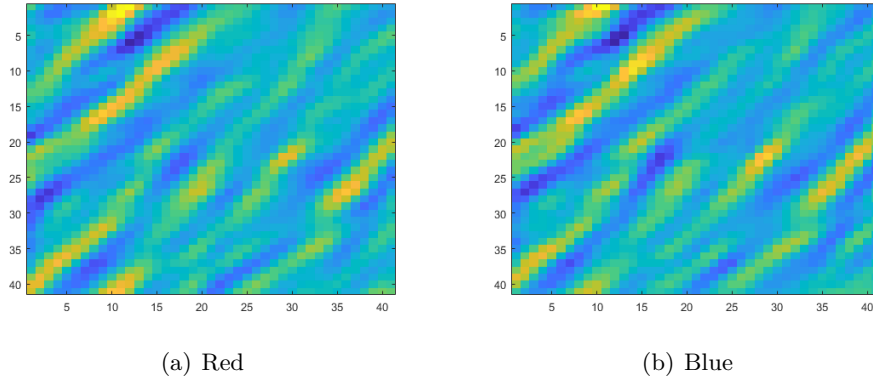


Figure 5.1.4: Radon filtering of Sentinel-2 image for each band. Comparison between red and blue bands to show the time lag. Zoomed to show it better.

5.1.2 Wavelet analysis application and bathymetry inversion

The wavelet analysis is now applied to the Sentinel data set. The results for the red band of the 8th date are shown.

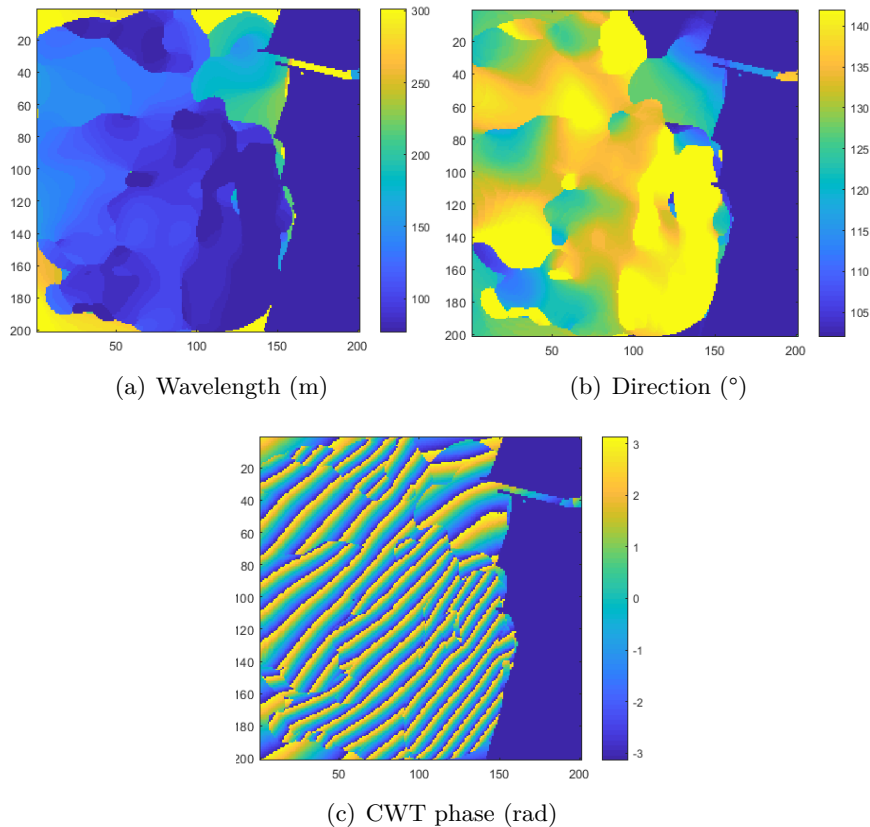


Figure 5.1.5: Outputs of the Continuous Wavelet Transform application to Sentinel-2 images.

First, it can be shown that the results are not valid at the mouth of the river, The wavelet method does not find a dominant wave there in the direction of the incoming waves, and instead it takes another peak. However, it is shown that the tendency of the wavelength is right:

it decreases as the waves approach the coastline. Moreover, the results near the border are not applicable due to the cone of influence of the wavelet transforms near to the borders of the image. The direction map of the waves have also a region of applicability, and the results correspond to the waves that were shown in the pre-filtered images. Finally, a map the phase of the CWT coefficients for the peak at each point are shown. If the method is well applied, the phase map should resemble the waves; and in fact, they are similar in the applicability region.

Next, by knowing the time lag between the red and green band, now the method can be applied to obtain the celerity as the wave displacement divided by this time lag, in the same way that is was done in the synthetic case. From the celerity values, the period is then calculated by knowing the wavelength distribution, and the depth is inverted by using the dispersion relation of linear wave theory. The results are shown in the following figure.

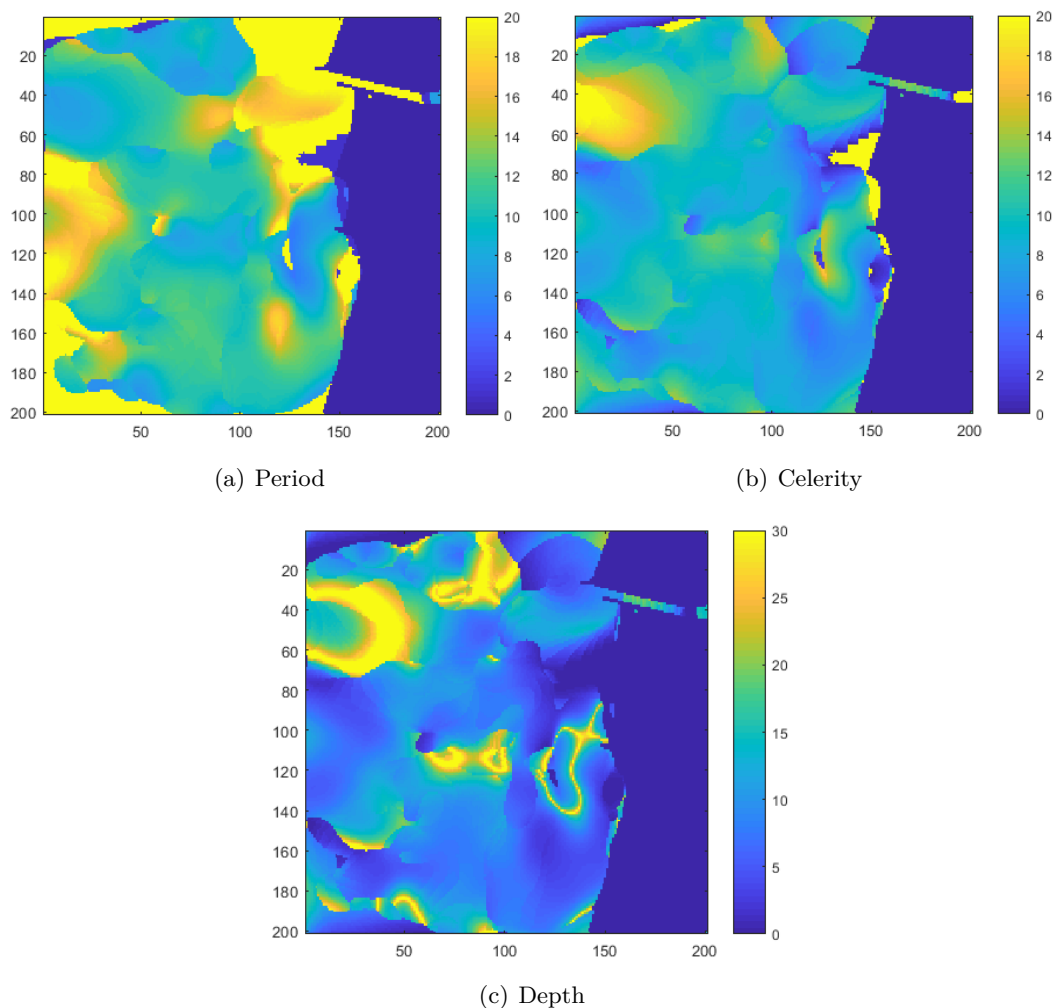


Figure 5.1.6: Map of wave properties of Sentinel-2 images and depth inversion.

The results of the celerity have also a region with high errors, but also a region where it is applicable. However, the results out of these region have values that are inside the range of possible celerity values. The same happens for the period. The values are more or less constant, as the period is conservative. The depth is then inverted and the results don't show a depth distribution, but they have the order of magnitude that we can expect by knowing the

Capbreton bathymetry. The results are influenced by the 10 m resolution of the image and the applicability of the method.

5.2 Pléiades

5.2.1 Data pre-filtering

After performing the analysis of all possible filters in the Sentinel-2 data set, it was decided to apply the FFT filtering with variable size windowing to the Pléiades images. The results will be shown to the first two acquisitions, as with only two images an estimation of the celerity can be done. In the next figure, the original and the filter images are shown.

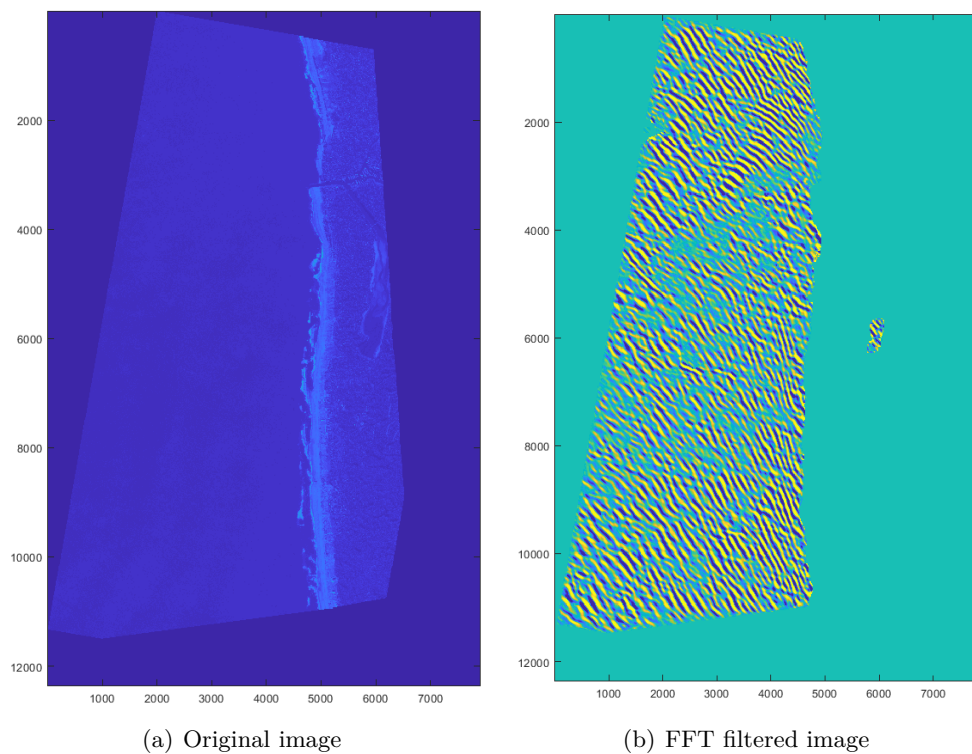


Figure 5.2.1: First Pléiades image of the video. Original and filtered.

In the next figure, a sub-sample of the image of the first and second dates are shown. If observed carefully, one could think that the waves are going backwards. In fact, is an effect of the data sampling, as with 8 seconds the waves has enough time to advance a distance greater than half of its wavelength.

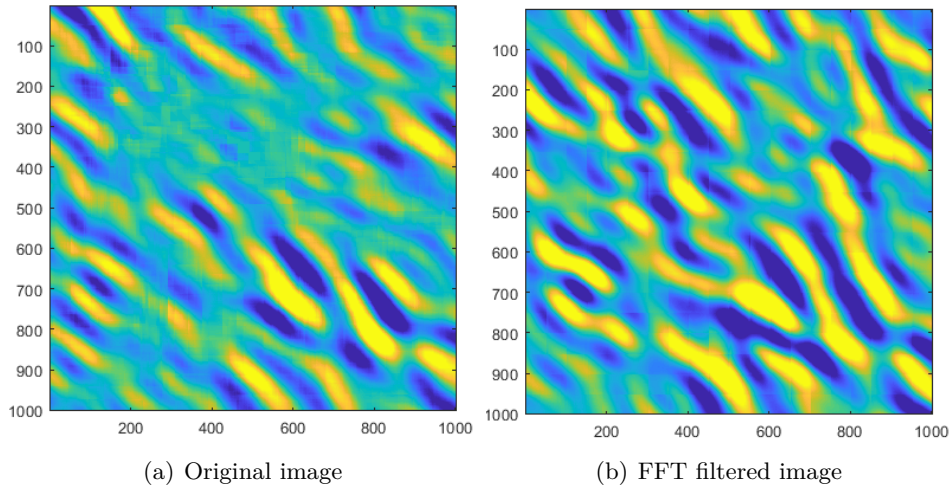


Figure 5.2.2: First and second Pléiades images of the video with the FFT filtering. Zoomed view

5.2.2 Wavelet analysis application and bathymetry inversion

The wavelet analysis is then applied to the Pléiades two first images. The results of the wavelet analysis for the first one will be shown. Because of memory issues in MATLAB, the CWT has been applied to bands of the image instead of the whole image at a time: that's why there is a band effect in the results. In order to avoid big matrices, as the original images have a size in the order of 1 GB, the wavelet analysis has been performed every 5m in wavelength and every 5° in direction.

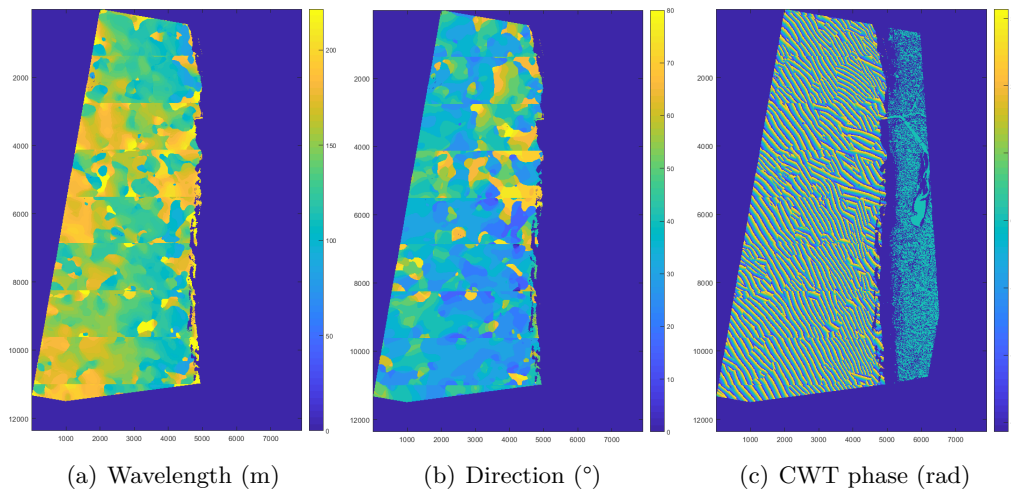


Figure 5.2.3: Outputs of the Continuous Wavelet Transform application to Pléiades images.

The wavelength maps are coherent with the wave theory, as it decreases near to the shoreline as for the Sentinel-2 results. The direction values are also in the order of magnitude instead in some regions where the algorithm has taken a peak in the CWT that does not correspond to the incoming wave. The CWT phase map is also quite coherent with the incoming waves.

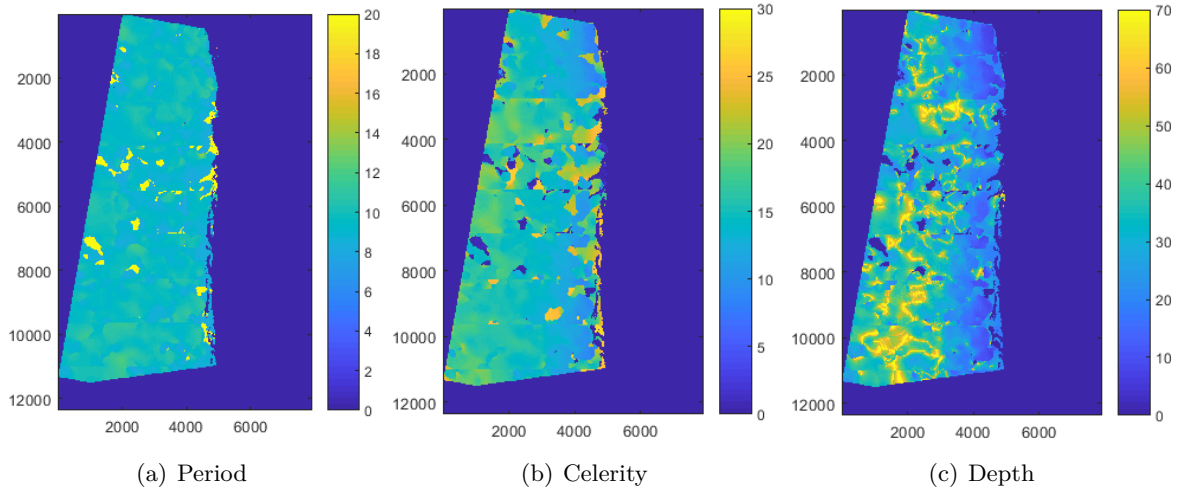


Figure 5.2.4: Map of wave properties of Pléiades images and depth inversion.

Finally, the periods, celerities and depths are calculated as for the Sentinel-2 images. It's also clear that there are some little regions where the analysis was wrong (the yellow zones in the period map), so the points out of these regions will be analysed. First of all, the period is constant in all the image, as the period is conservative, so that is an indication that the calculations there were accurate. The celerity exhibits also the tendency predicted by wave theory: the swallower (the nearer to the coastline) the slower. Finally, the depth tendency is also as it should be, being smaller near to the coast.

Chapter 6

Conclusions

The conclusions of this internship are listed:

- The Radon and FFT filtering produce similar results. However, the advantages of every method are different. In the Radon transform the angular precision is higher, whereas in the FFT filtering there is also a wavelength filtering.
- The filtering produced much better results if a method based on variable-size windowing, with smaller tiles near to the land or the image borders, is implemented.
- The wavelet algorithm has a great computational efficiency. However, it is limited by the size of the images, as there could not be enough memory in some computers. The solutions are to decrease the wavelength and direction ranges of the wavelet transform and to apply it in tiles, even if the power of the wavelet transform is lost, as it is not windowed and it is applied in the whole domain.
- For the finest resolution of 1m, in the Pléiades images, the results of the celerity are in the order of magnitude of wave theory. The depth calculation is limited by the applicability of the dispersion relation, as it can only be applied in intermediate depths.
- The application of this wavelet method to Sentinel-2 images gives celerity and depth values in the real order of magnitude, but its precision is limited due to the fact that the resolution is not metric and the time lag between bands is not very high, so the wave has little time to propagate. There could then be an accumulation of all these errors.
- The version of the CWT algorithm in which the peak of the spectrum for each point is taken as the dominant produces good results in the majority of the points. However, in some points the method fails as there could be a perturbation that is taken as a dominant wave, so in the spectrum it could be more than one peak.
- The wavelet method should be corrected in order to distinguish between the peaks associated with waves and the perturbations. Some ideas could be to take into account an spatial coherence or to add additional hypothesis to the method.

Chapter 7

Further work

The further works that will be done till the end of the internship and also the ones that would have to be done after it are listed:

- The wavelet method should be improved in order to take into account the several peaks of the spectra, in order to chose the relevant ones and not only the ones with greater coefficients.
- The methods will be, in the future, made GPU in order to increase the computational efficiency.
- The method will be used in regional or greater scales. In the future, it would allow to calculate a bathymetry estimation of the whole coast of Africa, for example.
- It will also directly applied to the Copernicus server, instead of downloading the data from Theia.
- Additional methods like cross-correlation will be compared to the wavelet method.
- A step beyond the wavelet method, in order to get results with less error and evaluate it, is the use of non-linear least squares fitting procedure in order to find the best-fit theoretical phase.
- The wavelet method will be applied to the whole Pléiades video instead of only two images, in order to obtain better results for the bathymetry.
- Apply an EOF to the Sentinel-2 data to obtain information from time.
- Results will be compared to real bathymetry.

Bibliography

- [1] Legos website. <http://www.legos.obs-mip.fr/>. Accessed: 2018-09-05.
- [2] Marcello De Michele, Sébastien Leprince, Jérôme Thiébot, Daniel Raucoules, and Renaud Binet. Direct measurement of ocean waves velocity field from a single spot-5 dataset. *Remote Sensing of Environment*, 119:266–271, 2012.
- [3] A. Poupardin, M. de Michele, D. Raucoules, and D. Idier. Water depth inversion from satellite dataset. In *2014 IEEE Geoscience and Remote Sensing Symposium*, pages 2277–2280, July 2014.
- [4] A. Poupardin, D. Idier, M. de Michele, and D. Raucoules. Water depth inversion from a single spot-5 dataset. *IEEE Transactions on Geoscience and Remote Sensing*, 54(4):2329–2342, April 2016.
- [5] Sentinel ii multi-spectral instrument (msi) technical guide. <https://earth.esa.int/web/sentinel/technical-guides/sentinel-2-msi/msi-instrument>. Accessed: 2018-08-18.
- [6] C. Danilo and R. Binet. Bathymetry estimation from wave motion with optical imagery: Influence of acquisition parameters. In *2013 MTS/IEEE OCEANS - Bergen*, pages 1–5, June 2013.
- [7] Rafael Almar, Philippe Bonneton, Nadia Senechal, and Dano Roelvink. Wave celerity from video imaging: a new method. In *Coastal Engineering 2008: (In 5 Volumes)*, pages 661–673. World Scientific, 2009.
- [8] Copernicus overview. https://www.esa.int/Our_Activities/Observing_the_Earth/Copernicus/Overview3. Accessed: 2018-08-18.
- [9] SUHET. *Sentinel-2 User Handbook*, July 2015.
- [10] Theia land data centre distribution portal. <https://theia.cnes.fr/atdistrib/rocket/#/home>. Accessed: 2018-08-18.
- [11] J. Donadieu and C. L’Helguen. Technical note. Sentinel-2A L2A Products description. Technical report, Centre National d’Etudes Spatiales, 2016. This document describes the SENTINEL-2A Level 2A products generated by MUSCATE.
- [12] GEO-Information Services EADS Astrium. *Pléiades Imagery User Guide*, October 2012.
- [13] Pléiades products. <https://www.intelligence-airbusds.com/geostore/>. Accessed: 2018-08-18.
- [14] Florence Sanchez and Marina Santurtun. Synthèse et analyse des données existantes sur un écosystème profond transfrontalier: le gouf de capbreton–«syntax». 2013.

- [15] Alaïs Mazières, Hervé Gillet, Bruno Castelle, Thierry Mulder, Corenthin Guyot, Thierry Garlan, and Cyril Mallet. High-resolution morphobathymetric analysis and evolution of capbreton submarine canyon head (southeast bay of biscay—french atlantic coast) over the last decade using descriptive and numerical modeling. *Marine Geology*, 351:1–12, 2014.
- [16] Capbreton’s port webpage. <https://www.cc-macs.org/economie/port-de-capbreton/cote-plaisance/le-gouf.html>. Accessed: 2018-08-10.
- [17] Stéphane Abadie, Rémi Butel, Sylvain Mauriet, Denis Morichon, and Hélène Dupuis. Wave climate and longshore drift on the south aquitaine coast. *Continental Shelf Research*, 26(16):1924–1939, 2006.
- [18] JM Jouanneau and C Latouche. Continental fluxes to the bay of biscay: Processes and behaviour. *Ocean and Shoreline Management*, 12(5-6):477–485, 1989.
- [19] Stanley R Deans. *The Radon transform and some of its applications*. Courier Corporation, 2007.
- [20] Peter Toft. The radon transform. theory and implementation. 1996.
- [21] Stanley R Deans. Hough transform from the radon transform. *IEEE transactions on pattern analysis and machine intelligence*, (2):185–188, 1981.
- [22] A. C. Copeland, G. Ravichandran, and M. M. Trivedi. Localized radon transform-based detection of ship wakes in sar images. *IEEE Transactions on Geoscience and Remote Sensing*, 33(1):35–45, Jan 1995.
- [23] Ran Su, Changming Sun, Chao Zhang, and Tuan D Pham. A new method for linear feature and junction enhancement in 2d images based on morphological operation, oriented anisotropic gaussian function and hessian information. *Pattern Recognition*, 47(10):3193–3208, 2014.
- [24] Mohamed Ali and David Clausi. Using the canny edge detector for feature extraction and enhancement of remote sensing images. In *Geoscience and Remote Sensing Symposium, 2001. IGARSS’01. IEEE 2001 International*, volume 5, pages 2298–2300. IEEE, 2001.
- [25] Lesley M Murphy. Linear feature detection and enhancement in noisy images via the radon transform. *Pattern recognition letters*, 4(4):279–284, 1986.
- [26] Michael van Ginkel, CL Luengo Hendriks, and Lucas J van Vliet. A short introduction to the radon and hough transforms and how they relate to each other.
- [27] Rafael Almar, Herve Michallet, Rodrigo Cienfuegos, Philippe Bonneton, Marion Tissier, and Gerben Ruessink. On the use of the radon transform in studying nearshore wave dynamics. *Coastal Engineering*, 92:24–30, 2014.
- [28] M. T. Rey, J. K. Tunaley, J. T. Folinsbee, P. A. Jahans, J. A. Dixon, and M. R. Vant. Application of radon transform techniques to wake detection in seasat-a sar images. *IEEE Transactions on Geoscience and Remote Sensing*, 28(4):553–560, July 1990.
- [29] E Oran Brigham and E Oran Brigham. *The fast Fourier transform and its applications*, volume 448. prentice Hall Englewood Cliffs, NJ, 1988.
- [30] NEELAM MEHALA and RATNA DAHIYA. A comparative study of fft, stft and wavelet techniques for induction machine fault diagnostic analysis.

- [31] Liu Chun-Lin. A tutorial of the wavelet transform. 2010.
- [32] Shi Yunhui and Ruan Qiuqi. Continuous wavelet transforms. In *Signal Processing, 2004. Proceedings. ICSP'04. 2004 7th International Conference on*, volume 1, pages 207–210. IEEE, 2004.
- [33] Ning Wang and Chungu Lu. Two-dimensional continuous wavelet analysis and its application to meteorological data. *Journal of atmospheric and oceanic technology*, 27(4):652–666, 2010.
- [34] Matlab 2d cwt documentation. <https://fr.mathworks.com/help/wavelet/gs/continuous-wavelet-transform-and-scale-based-analysis.html>. Accessed: 2018-08-17.